

Article

Understanding and Predicting Localised Variations in the Degradation Rate of Architectural, Organically Coated, Steel Cladding

Tim Savill *  and Eifion Jewell 

Materials Research Center, College of Engineering, Swansea University Bay Campus, Swansea SA1 8EN, UK
* Correspondence: 863047@swansea.ac.uk

Abstract: Organically coated architectural steel provides an economic, visually attractive, innovation friendly and robust building cladding. However, its performance, usually calculated using accelerated weathering and ‘artificial’ outdoor weathering testing, can be compromised within specific areas of the building envelope. The exact reasons for this are not fully understood. In an attempt to discern where and why performance varies, an investigation is carried out into some possible reasons for the performance discrepancy, and it is concluded that a combination of high humidity and the build-up of aggressive natural deposits contribute to high degradation rates in sheltered regions, such as building eaves, where microclimates are created. The build-up of deposits and their effect is presented as a key degradation accelerant during in-use service. A numerical simulation approach is developed to predict the natural washing, via rain impact and characteristics of the building analysed. This approach shows promise for determining areas unlikely to be naturally washed, and therefore subjected to a degradation accelerating, build-up of deposits. It is shown that such a simulation could be used to optimize the building design process to promote natural washing as well as provide an area-of-concern map in which exposed cut edge should be avoided and any manual inspection should be concentrated. It is also shown that nearby buildings can provide sheltering effects leading to decreased natural washing, increased deposit build-up and ultimately accelerated failure.

Keywords: organic coatings; degradation; corrosion; localised building conditions



Citation: Savill, T.; Jewell, E. Understanding and Predicting Localised Variations in the Degradation Rate of Architectural, Organically Coated, Steel Cladding. *Buildings* **2023**, *13*, 270. <https://doi.org/10.3390/buildings13020270>

Academic Editor: Oldrich Sucharda

Received: 6 December 2022

Revised: 11 January 2023

Accepted: 13 January 2023

Published: 17 January 2023



Copyright: © 2023 by the authors. Licensee MDPI, Basel, Switzerland. This article is an open access article distributed under the terms and conditions of the Creative Commons Attribution (CC BY) license (<https://creativecommons.org/licenses/by/4.0/>).

1. Introduction

Organically coated steel (OCS) panels are often used in industrial, commercial, and residential buildings as versatile cladding and roof solutions. They offer convenient and rapid installation, allow a variety of architectural finishes to be used, and provide designers a number of different aesthetic options through a wide variety of colour and gloss options. In fact, in 2020 approximately 38% of the 130 million tonnes of hot rolled steel produced in the EU, of which 5 million tonnes was organically coated, was used by the construction industry [1].

As the cladding makes up the outer protective skin and overall appearance of the building, it crucial for designers and owners to use OCS panels that will maintain both their structural and aesthetic qualities over the expected lifetime of the building, which can exceed 30–40 years [2]. As maintenance and replacement of panels is often dangerous, expensive, and difficult, it is important that the organic coatings are sufficient to protect the underlying steel substrate from corrosion and to maintain their visual appearance. The durability of OCS products is determined through the use of long-term natural exposure at sites with varying atmospheric conditions, and through the use of accelerated weathering techniques such as salt spray [3,4].

There are several different mechanisms by which OCS can degrade, which require different atmospheric conditions to be present. The most important environmental factors affecting the coating durability are light, solvents, temperature, humidity, mechanical

abrasion, and biological contaminants [5]. Light, specifically that in the UV range present in sunlight, can cause photooxidation and bond scission, which can increase the permeability and brittleness of the coating and reduce adhesion [6,7]. The most common solvent that affects OCS in use is water. Organic coatings are often porous to water and water can penetrate through flaws or defects present in coating systems, causing expansion and hydrolysis [7]. Presence of water can also lead to blistering and promote corrosion-driven failure mechanisms such as cathodic disbondment or anodic undermining [8–10]. The effect of these corrosion-driven failure processes can be greatly accelerated in the presence of salts and other aggressive compounds. Large temperature extremes can lead to softening, cracking, and increased brittleness, and large fluctuations can promote cracking and delamination [6,7]. Finally, in certain locations airborne particles can directly remove the coating if sufficiently susceptible, and biological contaminants may hold moisture and a variety of chemicals close to the coating surface or lead to the production of a differential aeration cell, which can accelerate corrosion [7,11].

Natural weathering testing is carried out by placing samples outside on racks and monitoring degradation during a period of up to 10 years (e.g., ISO 2810:2020 or BS EN 13523-19) whereas accelerated testing is usually a laboratory-based technique where the samples respond to aggressive environments such as salt-spray testing (e.g., ASTM B117 or BS EN 13523-8) or UV/condensation cycling (e.g., ISO 11507:2007 or BS EN 13523-10) [12–14]. It is important to note that the accelerated tests do not replicate atmospheric conditions and are typically used as a comparative tool to assess resistance between different products. Even though natural weathering sites are usually situated in harsh environments, such as marine or high UV and humidity, results can take years to gather due to the panel system technology. These extended test periods become a barrier to coating innovation and, subsequently, building design. Additionally, it is possible that the conditions at the test sites may differ from the proposed building site. Accelerated testing, such as salt spray or UV allows much quicker analysis of performance; however, the resulting analysis has to be viewed as an extrapolated result due to the artificial nature of the test, and it is often reported that accelerated results show poor correlation with field results [15,16]. Examples of a weathering rack and salt-spray tester are shown in Figure 1.

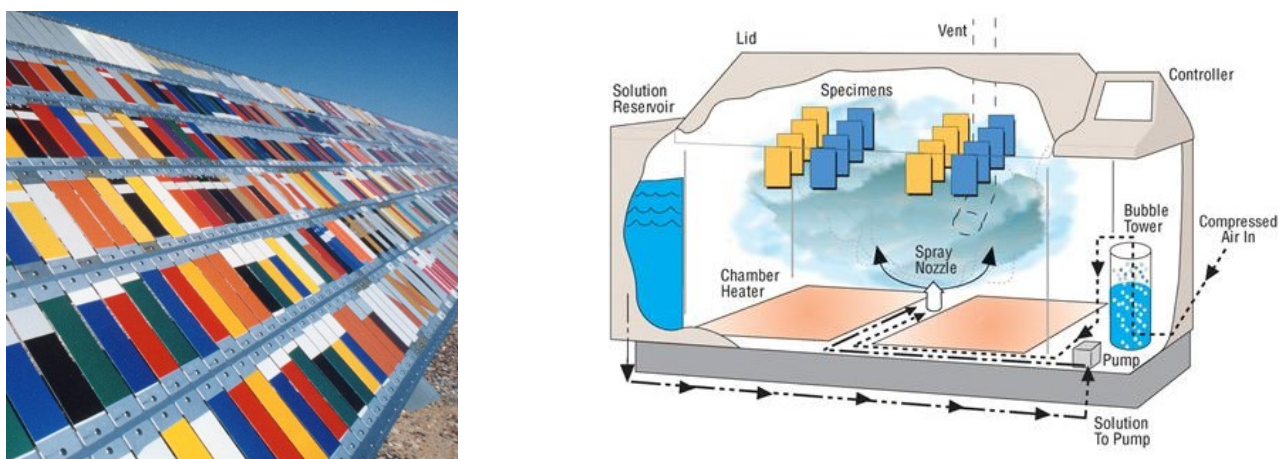


Figure 1. Outdoor weathering rack (left) and a salt-spray tester (right) [17,18].

Despite this extensive testing, more rapid failure of coatings is occasionally seen on buildings than the estimated performance would have suggested [19]. There has been some work to suggest that this is because the current tests do not always fully replicate the environment present in and on building façades due to geometries created as a result of modern building design principles and architecture [20]. For example, outdoor weathering racks, such as the ECCA T-19, expose relatively small samples at 90°, 45°, and 5° and although the 90° sample has a small overhang to produce sheltered regions,

this only extends 65 mm from the sample. In comparison, buildings will have far larger overhangs and alcoves, creating a much greater sheltering effect and likely producing more extreme microclimates. This is suggested by studies that have claimed that corrosion and delamination rate of paint both occur differently on a building compared to conditions of the standard racks [21].

The construction industry, in particular, is affected by the diverse environments in which OCS products are used. The use of accelerated weathering and natural exposure is well known; however, there is limited information regarding the effect of building design and its influence on the environments to which the OCS products will be subjected. Of particular interest is the determination of whether there are certain areas of buildings or building geometries that produce more localised aggressive conditions than those in standard tests, leading to accelerated failures. Such accelerated localised failures may lead to costly warranty claims against the OCS panel supplier associated with cost of reinstallation, reputational costs to architects and developers, and administrative and physical inconvenience to building tenants or owners. Thus, understanding both the likely location of and underlying mechanisms of such localised defects is critical to the entire OCS architectural supply chain.

This kind of work, considering how naturally occurring conditions affect performance, has been carried out previously for façades of different construction such as timber [22,23] and ceramic and renders [24–26]. However, it is not explored in great detail for OCS despite being highlighted as an important issue in other studies [4].

In this paper, a single-story building is examined to determine if localised accelerated degradation rates exist, the location of these, and the severity of the acceleration. An investigation was then undertaken to determine the factors contributing to this accelerated degradation with a consideration of localised microclimatic conditions and natural fouling deposits. The overall aim was to determine if it is possible to better determine and understand the conditions that cause accelerated degradation and use this information to predict areas of concern on a building. The end goal was to test the feasibility of developing a model that can be used to predict areas of concern across buildings for the purpose of design improvement and maintenance and inspection targeting.

2. Methodology

The strategy employed to study the relationship between potential failure of the OCS coating and localised conditions required a suitable building to be chosen. This building served to provide experimental data necessary to understand the mechanisms of degradation such as environment (both highly localised and ambient) and the role of accumulated fouling deposited on the building. Fouled samples could subsequently be taken for immediate laboratory analysis.

2.1. The Building: Materials and Locational Climate Data

The building used in this study is located on the Swansea University Bay Campus, Swansea, UK, as shown in Figure 2a,b, and is a one-story multipurpose teaching and office space that is mostly clad with polyvinylidene fluoride (PVDF)-coated steel panels. The building has a rectangular floor plan of 18 m × 12 m. The structural elements of the building are constructed from SIPS panels manufactured by Matrix structures and incorporate a transpired solar collector for thermal energy capture on the southern aspect and building-integrated PV on the roof for electrical energy capture, Figure 2a. The building was built in 2016 and the OCS is well within modern coated steel cladding lifetime warranties. The material characteristics are given in Table 1.

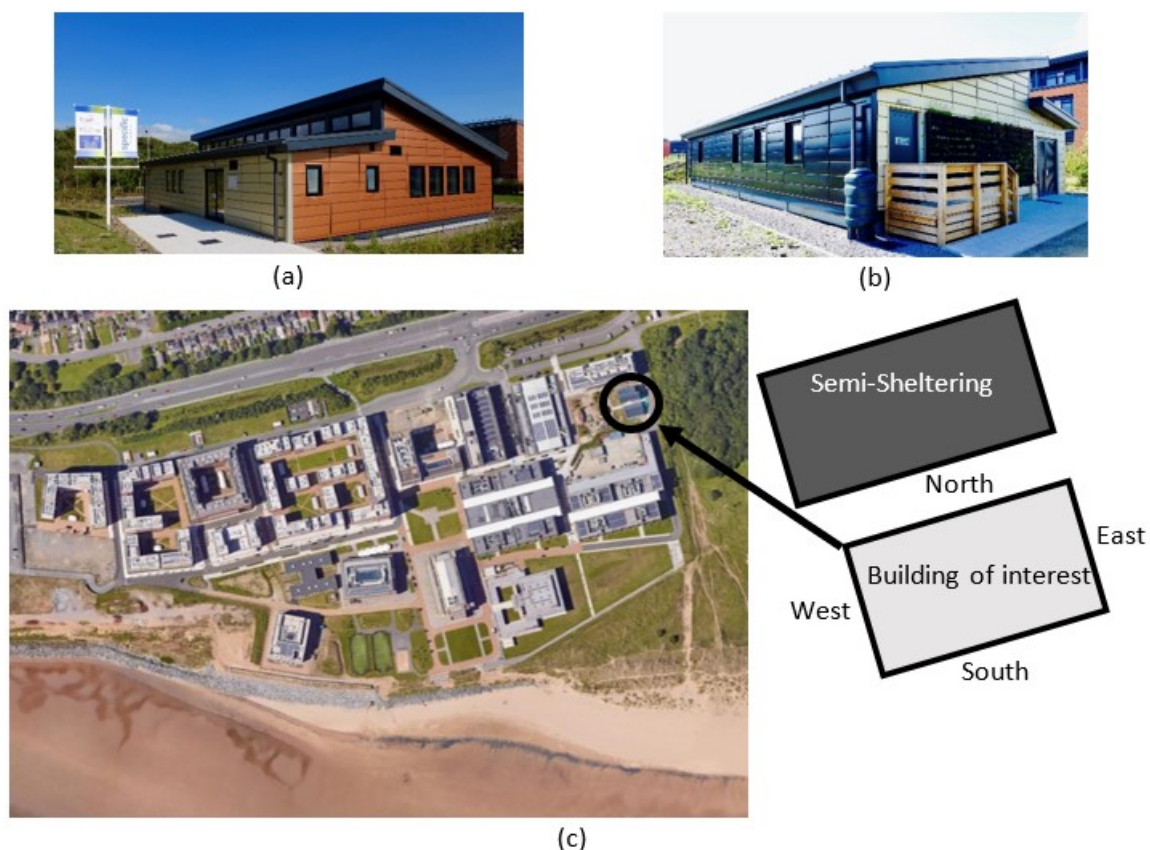


Figure 2. Building viewed from the (a) northwest, (b) southeast, and (c) location of the building and the façade names used for reference.

Table 1. Building material characteristics.

Structure	Material
Roof	Standing seam profile integrated PV and coated steel roofing
Main structure	SIPS panels attached to steel frame
External cladding (walls)	Interlocking plank profile PVDF-coated steel panels, attached via rail system
Cladding (soffit, guttering)	PVC-coated steel
Windows and doors	Glass and aluminium construction

The building is orientated slightly askew of cardinal points; however, can be said to have a north, west, east, and south aspect, as shown in Figure 2c. The location of the building is determined to be extremely corrosive with a classification of C4/5 according to ISO 9223. The key features of this location that make it a highly corrosive environment are the proximity to the sea (approximately 300 m due south), the M4 motorway (approximately 2 km due north), and various heavy industries (approximately 1–7 km southeast). It is also important to note that a building site exists directly adjacent to the west and south of the building and as a result the west side of the building was inaccessible during this work. There is also a small two-story building directly north of the building of interest that somewhat shelters the north face, which is important to note for later analysis in this work.

The average weather for this location (Table 2) indicates that this is a mixed environment that is slightly wetter and windier, yet sunnier than the UK on average.

Table 2. Average weather data for this location.

Metric	Location
Average temperature/°C	4.4–16.8
Average daily rainfall/mm	3
Average wind speed/ms ⁻¹	4.8–7.3

Wind rose

Average relative humidity/%	81
Average monthly sunlight/h	50–210

2.2. Experimental Tests

2.2.1. Measurement of Degradation

In order to measure the quantity of degradation across the classroom, a number of steps were involved with the first being a close visual inspection of the building. From this it was determined that generally the coated cladding was performing well and, in fact, the only sign of degradation was at the cut edge. This was to be expected as modern organic coatings are unlikely to experience thorough coating failure within 6 years following the building's construction, and cut edge corrosion is one of the most common routes of degradation for organically coated cladding [27]. Hence, the parameter measured to ascertain the degree of degradation was simply the distance from the cut edge that degradation had occurred. Measurement was carried out using digital callipers across a number of panels on each accessible façade of the building at different heights and locations, such as an alcove. The type of cut edge degradation was also noted with both blisters and white rust observed (both shown in Figure 3). Blisters are considered an early stage of cut edge coating degradation, whereas white rust is indicative of more severe metal substrate deterioration. At paint blister locations, water had penetrated the organic coating/metal interface and had reacted with the galvanised zinc surface causing a delamination separation of the metal and organic paint. This can ultimately lead to white rust formation when the zinc on the underlying galvanised metal surface is oxidised to zinc oxide.



Figure 3. Examples of the two main types of cut edge degradation observed: blistering (**left**) and white rust (**right**).

2.2.2. Collection of Highly Localised Microclimatic Data

Multifunctional sensors were developed to monitor the local atmospheric conditions that occur at various locations around the building façade. An Arduino pro mini was used along with multiple sensors to provide low cost, easily manufacturable devices capable of measuring a diverse range of atmospheric conditions, which are given Table 3. While the absolute calibration of each device to relevant SI standards is not quantified, the repeatability of each sensor type provides satisfactory relative measurement. Each multifunction measuring unit had a footprint of only 20 cm × 10 cm × 5 cm allowing them to be magnetically attached within a small defined area on the building façade. Each unit was battery operated and could measure continuously at 4 readings per hour for 4 weeks. Data could subsequently be transferred via SD card and the battery replaced within 5 min thus allowing for continuous measurement.

Table 3. Sensors used in the multifunctional sensing device.

Parameter	Sensor	Operational Principle	Quoted Repeatability
Air temperature	Adafruit BME 680	Diode Voltage	±1 °C [28]
Humidity	Adafruit BME 680	Capacitive	±3% [28]
Panel temperature	Adafruit TMP 006	IR Thermopile	±1 °C [29]
UVA	Adafruit VEML 6075	Photodiode	±3 μWcm ⁻¹ [30]
UVB	Adafruit VEML 6075	Photodiode	±3 μWcm ⁻¹ [30]
Particulate concentration	Grove PPD42NS	Low Pulse Occupancy	±50% [31]
Time of wetness	Grove Capacitive Moisture Sensor	Capacitive	±5%

Five of these multifunctional sensing boxes were used in this work and these were deployed to observe if significant variations in conditions exist between low, middle, and high locations on a façade and for different façades. To this aim, three boxes were placed on the north face of the building at ground level, mid-way up the façade, and in the eaves; two boxes were placed on the south face at mid-way up the façade and in the eaves. These locations are given in Table 4 and shown schematically in Figure 4. Data were collected from September 2020 to September 2021 at a rate of four measurements per hour.

Table 4. Sensing box locations and their properties.

Number	Façade	Height	Location Type
1	South	Middle	Exposed
2	South	High	Sheltered by roof overhang
3	North	Low	Exposed/semi-sheltered by 2nd building
4	North	Middle	Exposed/semi-sheltered by 2nd building
5	North	High	Sheltered by roof overhang/semi-sheltered by 2nd building

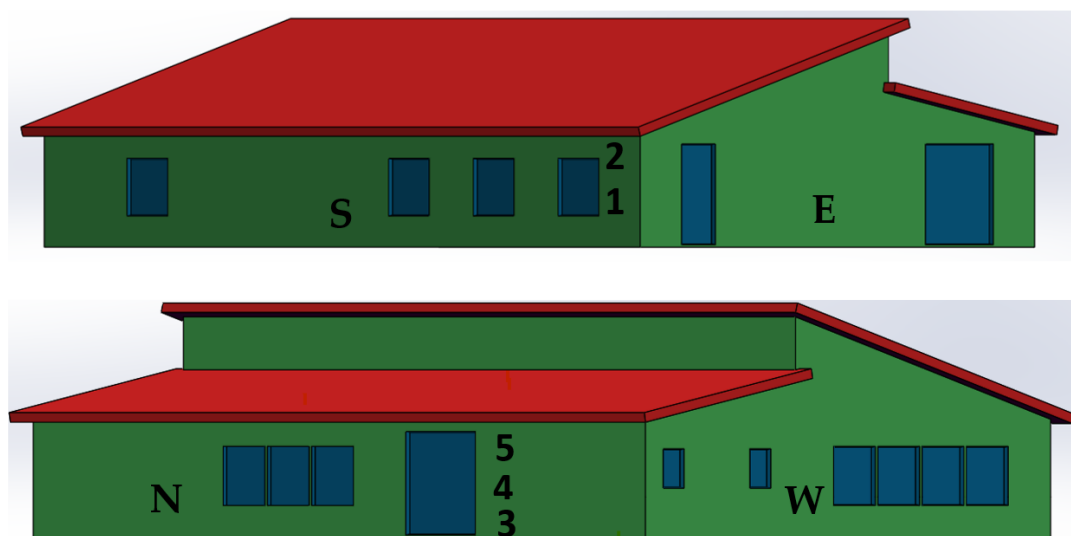


Figure 4. Location of the five sensing boxes on the building. The building is coloured according to materials with green indicating PVDF cladding, red indicating integrated PV roofing, blue indicating windows and doors, and dark purple indicating the soffit region composed of PVC cladding material.

2.2.3. Collection, Measurement, and Analysis of Accumulated Natural Deposits

The deposit accumulation was studied in two different ways. The first was to sample a fouling deposit from the building for subsequent laboratory analysis to establish the components of the deposit and hence the likely effect of its presence on OCS degradation. The second examined how the presence of the deposit on the OCS could affect the wetting and moisture retention properties leading to the creation of conditions which are amenable for degradation. This was facilitated by the production of fouled samples in the laboratory using the deposit collected from the building. Novel sampling methods were developed in order to obtain a repeatable measurement of the deposit found at each location and to distinguish between the solid matter and the soluble compounds present, both of which could contribute to the degradation of the OCS.

The procedure to measure the quantity of deposit in each location was as follows. First, a plastic sampler guide with a 5 cm × 5 cm square hole was attached to the location and this area was swabbed using a foam-tipped bud until all the deposit present had been collected. This bud was then placed in a weighing boat with 5 mL of deionised water and washed until all the deposit was transferred to the boat. The boat was then placed on a hot plate at 50 °C for 3 h at which point all the water had evaporated and only the deposit remained. The boat was then weighed, and this weight was compared to the pretest weight to calculate the deposit weight. For each location, three repeats were carried out and a control weight boat, with no deposit added, was used to ensure no weight loss was experienced simply by heating the weighing boat. Once an average for each location was calculated, this was converted into a value in mgm^{-2} based on the original sampling area size.

In order to analyse the composition of the deposit, 5 cm × 5 cm 4-ply nonwoven sterile swabs were used to collect a significant amount of matter from the building whilst wearing nitrile gloves. The gauze was placed in 200 mL of deionised water for approximately 2 days to ensure any absorbed matter was removed. After the two days, the gauze was removed using plastic tweezers and examined to ensure that the deposit had been removed. The gauze was wrung and left to dry to allow any further matter to be extracted. The resulting solution was passed through filter paper. This filter paper was removed and placed in a Petri dish on a hot plate at 50 °C for approximately 3 h to dry the powder. The powder was then collected and placed in a clean sample box. A separate swab was taken of the building and this swab was dried in a similar manner and the dry powder was then scraped off the gauze into a clean sample box. This gave two lots of dry powder for examination, one that should have any soluble components removed (P, particulates) and the other as was found on the building façade (SP, soluble compounds, and particulates).

The solid particles obtained via the collection methods were characterised using energy dispersive spectroscopy (EDS) in a Hitachi TM3000 Desktop scanning electron microscope (SEM). For each sample, three different areas were examined and an average atomic weight % calculated from these results. As there were a number of particle sizes, the three areas chosen covered a variety of particle sizes and shapes. Further analysis to determine the chemical constituents of compounds present was carried out using X-ray diffraction (XRD) [32].

The conductivity of solutions formed using the collected natural deposit was measured using a custom-made solution conductivity device. This was composed of a square plastic container with two 1 cm diameter cylindrical graphite electrodes protruding in from opposite sides and fixed with a 1 cm gap between them. The resistivity of the solution added to this setup was measured and converted into the conductivity. The temperature of the solution was monitored and used to adjust the conductivity to the commonly used 25 °C conductivity value to ensure comparable results. This setup was calibrated with several concentrations of NaCl in deionised water with known conductivity values.

2.2.4. Creation of Laboratory-Fouled Samples and Analysis of Moisture-Related Properties

In this work, the effect of natural deposit build-up was examined on a number of commonly used organic coating systems for steel cladding, namely a PVC-based system, a PU-based system, and a PVDF-based system. Samples 5 cm × 5 cm in size were used to create the fouled samples; 5 and 10 mg of building deposit was added to each sample to give two samples with a deposit coverage of approximately 2000 and 4000 mgm⁻², respectively. The deposit was dissolved in approximately 5 mL of deionised water and was pipetted onto the sample and allowed to dry on a hot plate at 50 °C. This produced visually similar fouling to that observed on the actual building, as shown in Figure 5. To ensure this process did not affect the results, the clean samples also went through the same procedure of water addition and heating.



Figure 5. Initially clean PVDF sample (left), PVDF sample with wet-applied 4000 mgm⁻² of deposit (middle), and observed natural deposit on the building (right).

Measurement of the wetting angle of the laboratory-fouled samples was carried out using a contact angle measurement system composed of a mounted pipette and camera. One droplet of deionised water was expelled from the pipette onto the sample surface, which was recorded using a camera and the resultant contact angle calculated using FTA 32 software (First Ten Angstroms, Newark, USA). The measurement was repeated at different sites on the sample surface three times with an average taken from these measurements.

The moisture retention of the fouling deposit from localised microclimates was considered to be a possible contributory factor in the degradation of the OCS. An experimental method was developed that allowed for this to be investigated in the laboratory by placing fouled samples in a controlled humid environment, Figure 6. This was composed of a sealed tub partially filled with a 5 wt.% NaCl electrolyte to maintain a humidity of 95%. The samples were placed on a plastic stage that was supported and held out of the electrolyte by using plastic supports. The three samples of each coating system with deposits representing 0, 2000, 4000 mg m⁻² were first weighed and then placed in the chamber. They were then removed and reweighed periodically to measure weight change as a result of moisture absorption onto the surface. After the final weight was recorded, the samples were also photographed to allow visual observation of any changes.

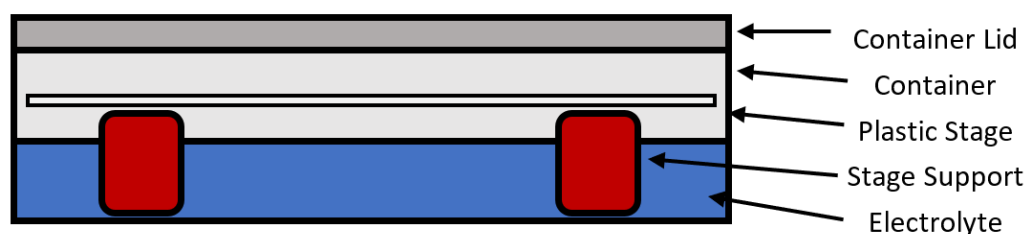


Figure 6. Experimental setup of the humidity testing chamber.

In order to measure the effect of deposit presence on the retention of water and the drying rate of the laboratory-fouled samples, each sample was weighed and then nine 5 μ L drops of deionised water were placed on the sample, as shown in Figure 7. The samples were left at room temperature and reweighed every 10 min until the weight of the sample returned to that of the original state. The weight of water present on the samples was then calculated for each time step.

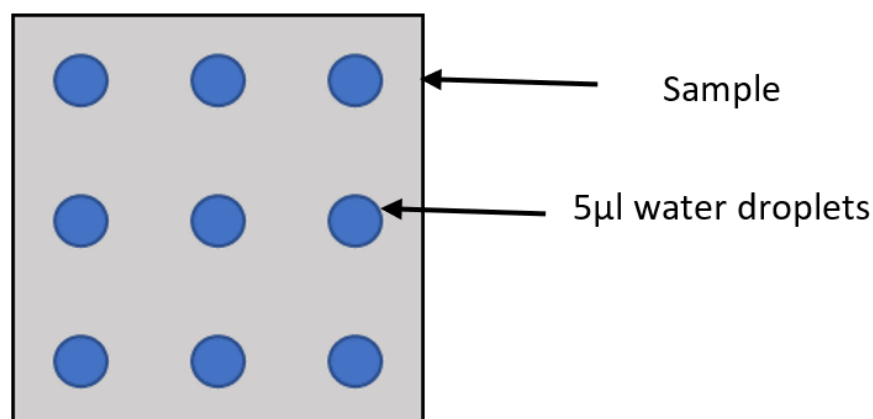


Figure 7. Droplet test used to measure drying/water retention.

2.3. Numerical Simulation of Rainfall

The aim of the rain impact simulation was to develop a theory that accurately describes the experimental observations and to identify possible mechanisms for variations in the highly localised microclimates around the building that could influence OCS panel degradation. Potentially, those areas where air flow is limited may maintain a localised

humid atmosphere, while areas which see negligible rain impact are less likely to have deposit fouling removed. Ultimately, the building simulation was seen as a means of providing a predictive tool that could be used to identify areas where potential OCS panel degradation would be accelerated. This would allow for refinements to be made at the design stage, investigate best practice for design, or apply warranty limitations for OCS used in specific areas of the building. As these are building design, local environment, and meteorologically linked, it is envisaged that such simulations would ideally be required for each location.

The building was created as a scale 1:1, 3D object in Solidworks 2022 using both the original architectural plans and physical measurements to ensure accurate building dimensions were used. To reduce the computational demand, small details such as the joints between panel sections, guttering, and other such features were not included in the model; however, larger features such as doorway and window surrounds were included. The building model is shown in Figure 8.

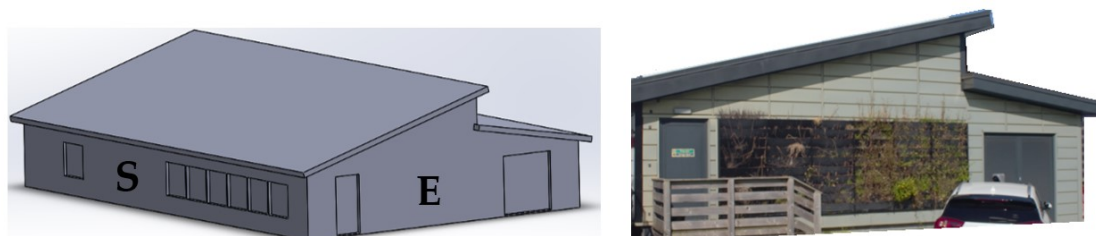


Figure 8. Building model (left) and actual building (right).

The nearby building providing sheltering was similarly modelled but, to reduce computational demand, less detail was used as it was only included to show the effect of a nearby sheltering building. This simple model was then, when required, placed as measured in relation to the building model, as shown in Figure 9.

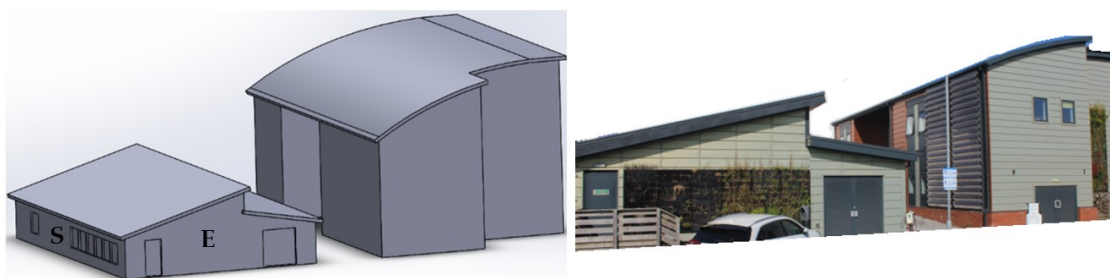


Figure 9. Dual building model (left) and actual buildings (right).

Both models, with and without the second building, were surrounded by a bounding box which extended in all directions by 60 m from the model and was 10 m and 20 m tall for the single and double building models, respectively. Extending the solution significantly beyond the area of interest ensures that the structures have a negligible effect on the domain boundary conditions

Meshing was carried out using ANSYS meshing with a face sizing of 150 mm on the building, a maximum size of 10 m, and a growth rate of 1.25. The final mesh had approximately 100,000–120,000 nodes, which varied for the different systems used.

The simulations were carried out using ANSYS CFX, general purpose CFD software (ANSYS, Canonsburg, USA), which utilises a finite-volume method solver and the Reynolds-averaged Navier–Stokes (RANS) equations. The $k-\epsilon$ turbulence model was used with scalable wall functions assuming a nominal 10% turbulence intensity at the inlet flow. The simulation was run isothermally (at 25 °C), but did include buoyancy effects with gravity defined in the Y direction as -9.81 ms^{-2} with a buoyancy reference density equal

to that of the density of air at 25 °C, 1.19 kgm^{-3} [33]. One-way coupling was enabled so that droplet trajectories were influenced by air flow, without the change in droplet momentum influencing the air flow. Similarly, droplets did not interact with each other, so each droplet's path was considered statistically independent. A droplet drag coefficient of 0.5 was attached to the rain particles, which assumed a spherical shape for raindrops [34].

The fluid domain contained air at 25 °C that was modelled as a continuous fluid and water that was modelled as a particle transport solid with a diameter influenced by number particle distribution. This was defined using a minimum diameter of 0.1 mm and a maximum of 4 mm with a mean particle diameter of 1.5 mm and standard deviation of 1 mm. The particle diameter directly influences its trajectory through its mass and drag. It has been shown that rain particle diameter does vary as a function of rain intensity and a number of other environmental factors [35]. However, based on similar simulation work, it was thought that this provided a suitable foundation for experimental work [35]. RTP condition (25 °C) was used for the domain temperature for simplicity and because the temperature would have little effect (apart from very slight density differences), as the CFD model does not model interactions between mass transfer mechanisms between the liquid droplet and the air.

The computational domain is shown in Figure 10 and had the following boundary conditions set: the upper face 'sky' boundary was set as an opening with 0 Pa relative pressure with random injection of water particles from approximately 600,000 injection regions. The inlet location varied depending on the desired wind direction for each test; however, each inlet was defined to have a normal air velocity varying from 2 to 12 ms^{-1} , representing a range of local wind conditions (Table 2). All other boundaries were set as smooth walls with a restitution and parallel coefficient of 0 to draw attention to the areas that rain impacted the building, i.e., when droplets hit the surface, they stick, and their path is considered ended. No consideration was given to the droplet's formation on the surface or the subsequent dripping through the action of gravity. The droplet flow rate was such that total droplet volume represented the annual rainfall. All other boundaries were set as smooth walls with a restitution and parallel coefficient of 0 to draw attention to the areas that rain impacted the building.

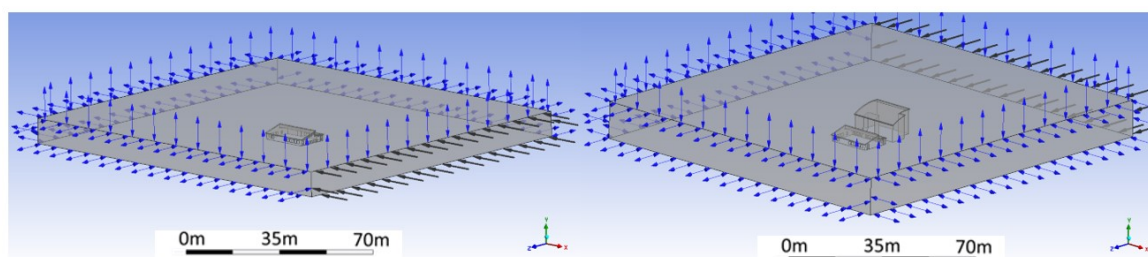


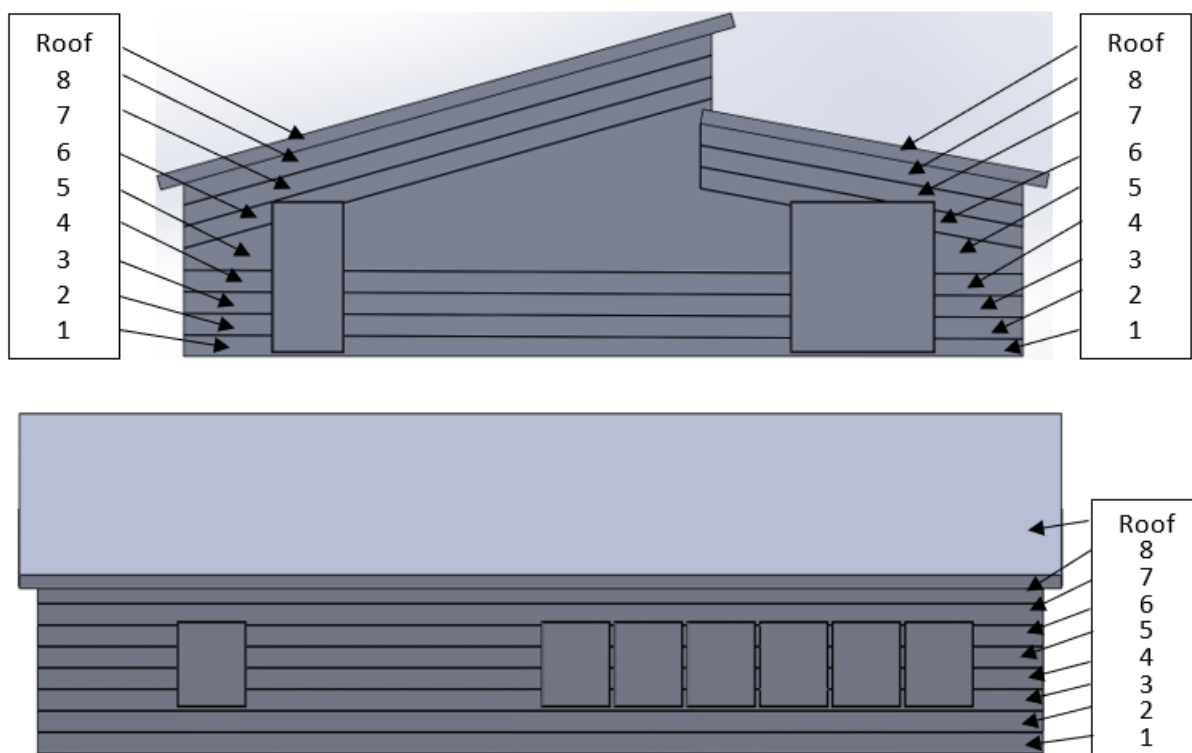
Figure 10. The computation domain for the single (left) and dual building (right) models. The black arrows signify an inlet boundary condition whereas the blue arrows show an open boundary condition.

The fluid simulation models were carried out in two strategic steps. Firstly, the single building model was examined with wind applied at the north, south, and east elevations to understand the effect of building geometry on rain (particulate) impact distribution and the relationship with natural fouling. These wind directions represent approximately 19%, 22%, and 23% of the wind experienced in this location, respectively. Secondly, the effect of the adjacent, 'semi-sheltering', building in close proximity was then examined for the rain impact on the north face from northerly winds. The simulation scenarios are described in Table 5.

Table 5. Simulation scenarios.

Scenario	Model Used	Wind Direction	Wind Speeds Used ms^{-1}
1–11	Single building	From east	2,3,4,5,6,7,8,9,10,11,12
12–22	Single building	From south	2,3,4,5,6,7,8,9,10,11,12
23–33	Single building	From north	2,3,4,5,6,7,8,9,10,11,12
34–44	Dual building	From north	2,3,4,5,6,7,8,9,10,11,12

Any CFD simulation is capable of producing a large volume of data on the fluid flow. However, in this instance it is the impact of the fluid flow on the rain impact density that is critical to understanding how the rain could influence the removal of fouling deposit. Semi-quantitative data were produced by sectioning the façade into a number of regions 300 mm in height to mimic the locations measured on the actual building. An example of this sectioning is shown for the south and east faces in Figure 11 and shows the sections numbered 1–8 increasing in height from the floor to the roof. For the east face, panel Section 5 is much larger to account for the slope and presence of both roof sections; however, it gives a representation of a section approximately the correct height from both floor and roof. For each section, the quantity of rain impacting that region was recorded as an average volume fraction, averaged across the area of the section. This was to complement the visual analysis of the results.

**Figure 11.** Example of façade sectioning for the east (**top**) and south (**bottom**) façades.

3. Results—Physical Experimental Work

The results of this work are presented in two separate sections that describe the physical measurement of the building and the simulated results. This section, covering the physical results, begins with an assessment of the measured degradation severity across the building to establish which general regions show evidence for experiencing higher degradation. The measured environmental conditions for a number of locations are then provided to discuss trends in the conditions present in different locations and

suggest correlations of these conditions to the varying levels of degradation. The variation in build-up of natural fouling deposits is then presented and compared to the observed degradation levels. The likely effect of fouling on degradation is examined by presenting the constituents of the deposit and the effect of fouling on key features, such as water contact angle and time of wetness.

3.1. Degradation Variations across the Building

The observed cut edge defect distance across various locations on the building is shown in Figure 12. Generally, the east and south façades showed similar levels of performance; however, far greater degradation was observed on the north face. Equally, it was observed that distance and severity of cut edge corrosion increased with the height of the panel with far more significant cut edge degradation occurring in the panels mounted high in the eaves of the building than those at ground level for all observed façades. Initially, degradation is observed as blistering, which initiates corrosion and formation of white rust, which is in line with the literature [6]. This trend was also observed in door and window regions. The soffit region displayed moderate defect size, although this region was composed of more durable PVC-based coated material; hence, this may explain why it was perceived to be performing better than the highest PVDF panels that are in close proximity to the soffit region.

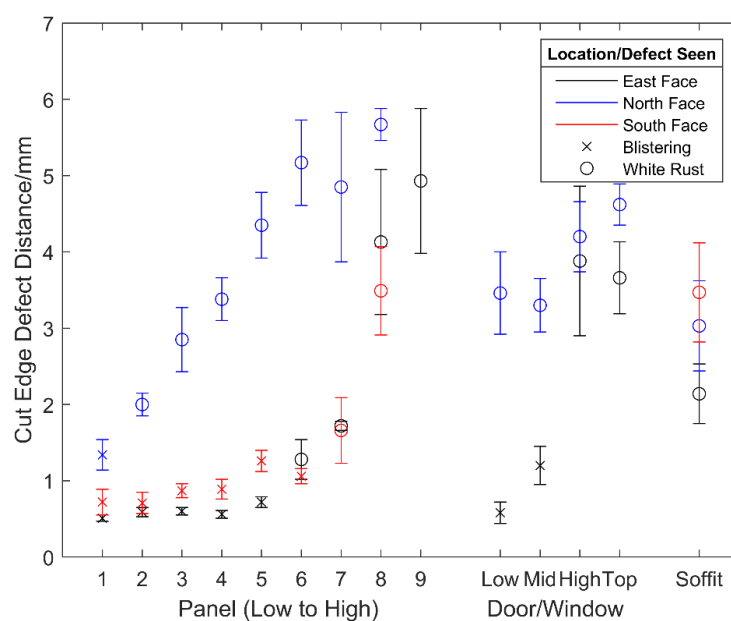


Figure 12. Variation in cut edge defect size and type across the building.

These results suggest that performance is significantly different across the building and even between regions separated by a few meters. When considering the age of the building, the level of degradation seen in certain locations is considerable; amounting to around 1 mm of cut edge corrosion per year. While it is possible that the discrepancy in performance is due to other factors, such as variance in workmanship or installation, the initial hypothesis was that this was a result of microclimatic aggressive localised conditions.

3.2. Environmental Condition Variations across the Building

3.2.1. Temperature

The temperatures measured through the year reflect those which would be expected in a UK coastal location. Both the recorded ambient temperature and the panel temperatures, Figure 13, were generally fairly similar across all the locations with variations limited to a maximum of 3–4 °C. Location 1 (south middle) experienced the highest temperature fluctuations due to it being on the south face and with greater sun exposure. This region also

experienced some of the lower temperatures in the winter months. The panel temperatures follow a similar trend to the ambient temperature but are on average approximately 3 °C lower. This is attributed to radiative heat losses experienced during the measurement process of the IR thermopile sensor.

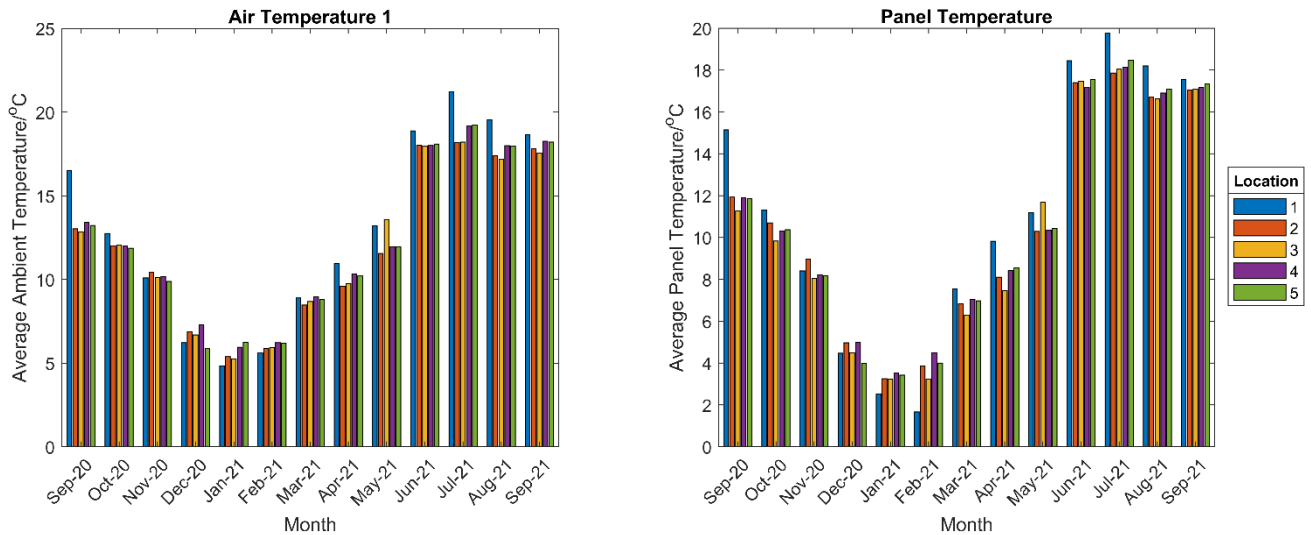


Figure 13. Comparison of air (left) and panel (right) temperatures recorded at each location.

3.2.2. Humidity

The measured humidity at each site, shown in Figure 14, shows much more variation among locations. Of particular interest is the difference between those locations that are high up in the eaves and are considered sheltered locations (2,5) and those lower down, which are far more exposed to the elements (1,3,4). Although there was some variation, on average these high locations recorded 4–5% increased relative humidity during the test period.

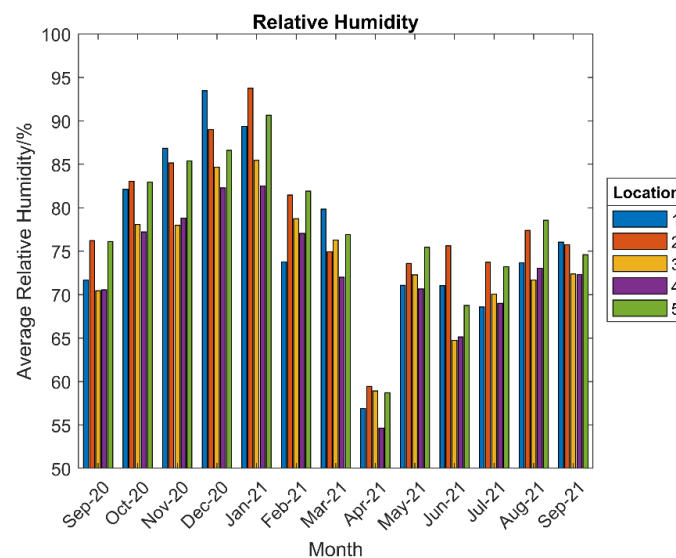


Figure 14. Comparison of the relative humidity recorded at each location.

3.2.3. UV Exposure

As expected, the recorded UVA and UVB intensity at each site, shown in Figure 15, shows that the high locations receive far lower irradiance by UV than the mid and low regions due to the roof overhang providing shade. Furthermore, the exposed south-facing

location (1) received the highest UV exposure, which is consistent with sun movements for the northern hemisphere.

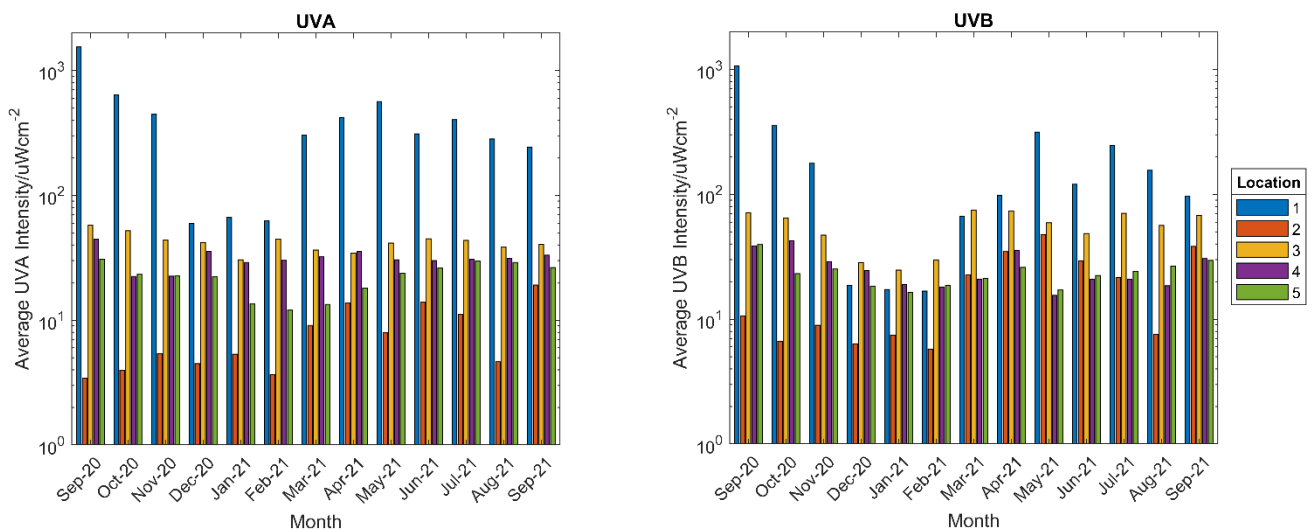


Figure 15. Comparison of UVA (left) and UVB (right) intensity recorded at each location.

3.2.4. Time of Wetness

The measured time of wetness at each location was calculated by comparing the number of readings captured suggesting probe wetness over 10% to those suggesting probe wetness under 10%. In Figure 16, it is observed that generally sites 1 and 2 showed greater wetness than the other sites. It is thought this is because sites 1 and 2 are more exposed to wind-driven rain than the north sites due to the semi-sheltered nature of the north face due to the building closely situated adjacent to the north. As expected, owing to increased rain exposure, comparing the mid and low sites to the counterpart high sites, the more exposed lower sites showed greater wetness. However, the high time of wetness of site 2 shows that just because a site is high and sheltered by the roof of a building does not necessarily preclude it from moisture build-up related to factors such as humidity.

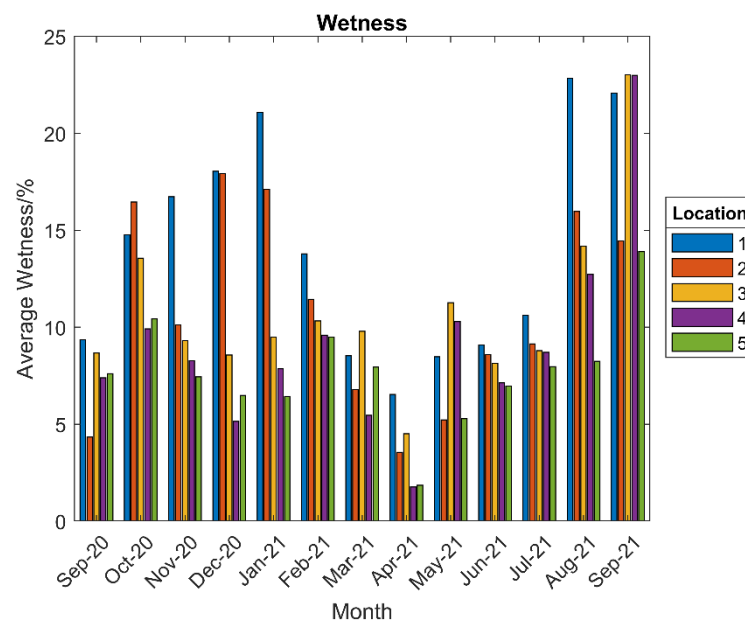


Figure 16. Comparison of % wetness recorded at each location.

3.2.5. Airborne Particulate Concentration

Figure 17 shows the measured particulate concentration at each location from which it is observed that there appear to be few obvious trends, although it can be said that higher average concentrations were observed on the lower, more exposed regions. It is thought this is because these locations experience the greatest exposure to wind, and hence more particles are wind-driven towards these areas. However, it is important to note that the number of particles arriving at a location does not always correlate with the amount of deposit building-up due to variations in natural washing across the building.

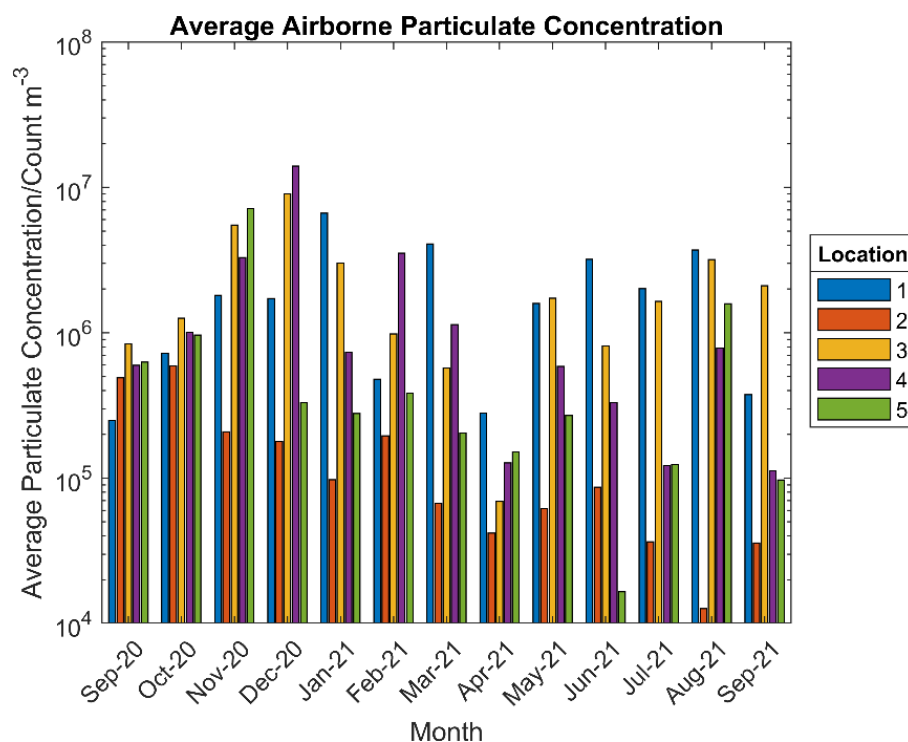


Figure 17. Comparison of particulate concentration recorded at each location.

3.3. Variations in Natural Deposit Build-Up across the Building

The calculated weight of natural deposit built-up at each building location is shown in Figure 18. Generally, the north façade shows greater deposit build-up than the east and south, which show similar levels. Furthermore, the amount of deposit present increases from low at ground-level panels to the highest at the panel in the eaves of the roof and similarly increases in the door and window surrounds. The soffit regions showed relatively low levels of deposit build-up. Comparing the data presented in Figure 18 to that of the cut edge defect data shown in Figure 12, it is evident that increased natural deposits correspond to increased cut edge defects and white rust.

To compare the correlation visually, the deposit weight was plotted against the cut edge defect distance, Figure 19, and a positive, nonlinear trend was observed. It was also observed that blistering only occurred in locations where the deposit weight was lower than approximately 250 mgm^{-2} , with white rust observed at all locations with larger deposit weights. Figure 19 also displays that the trend can be approximated to logarithmic with a calculated Pearson correlation coefficient of 0.92. The strength of the correlation led to discarding the idea that the performance variation could only be down to an additional factor such as poorer workmanship and installation in these regions.

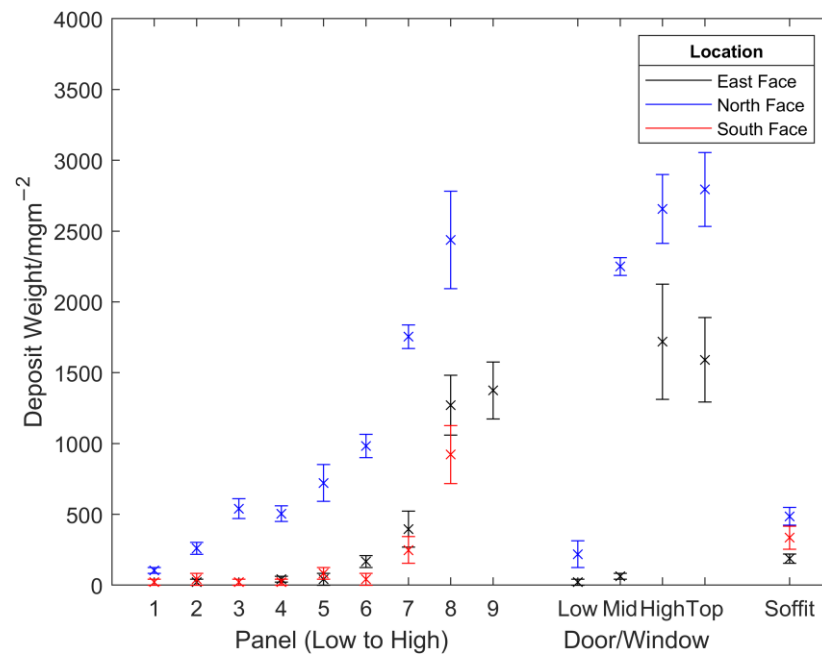


Figure 18. Variation in the amount of deposit present across the building.

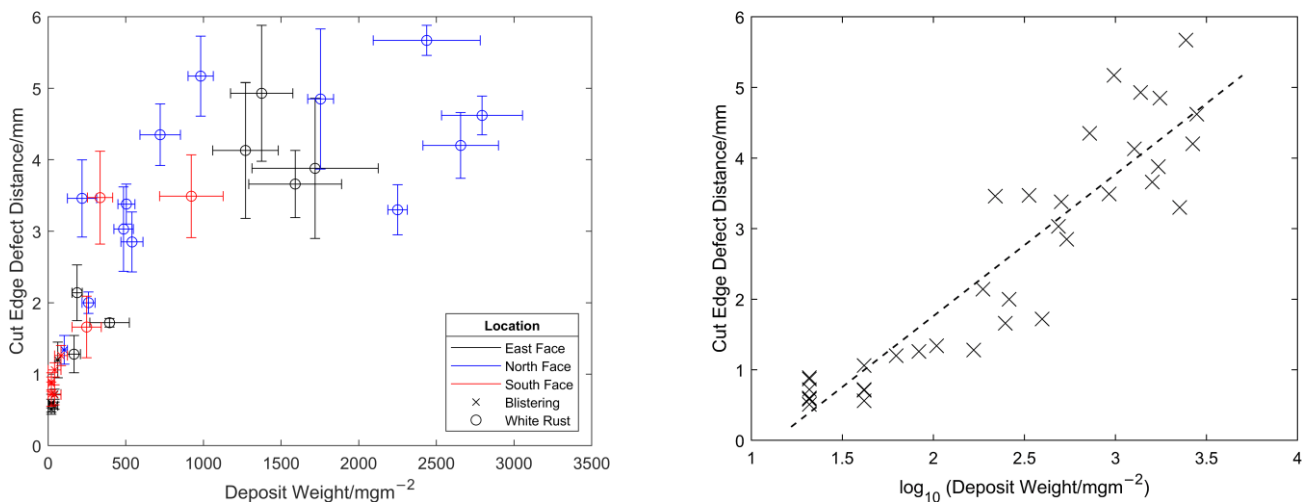


Figure 19. Comparison of the cut edge defect distance to the measured deposit weight in each location (left) and a demonstration of the logarithmic trend between the two factors (right).

3.4. Analysis of the Naturally Occurring Deposit

Figure 20 shows the results of the EDS analysis of the natural deposit samples SP and P. A variety of elements are present in both samples and the weight % of those often expected to be present in soluble compounds decreases in the P sample, where dissolution would have likely occurred. Of particular interest is the presence of chlorine, which appears to be soluble, presumably as Cl^- , which contributes to accelerated corrosion.

The EDS% weight data were used in combination with the likely compounds present, matched with the XRD results, Figure 21, to identify the compounds and the likely percentage distribution of these compounds in the two samples. The resulting data are displayed in Figure 22. Again, it was observed that water-soluble compounds are less prevalent in the P sample, as would be expected. It is worth noting that not all elements identified in the EDS work formed part of a compound in the XRD analysis, suggesting other compounds composed of the unmatched elements may also be present.

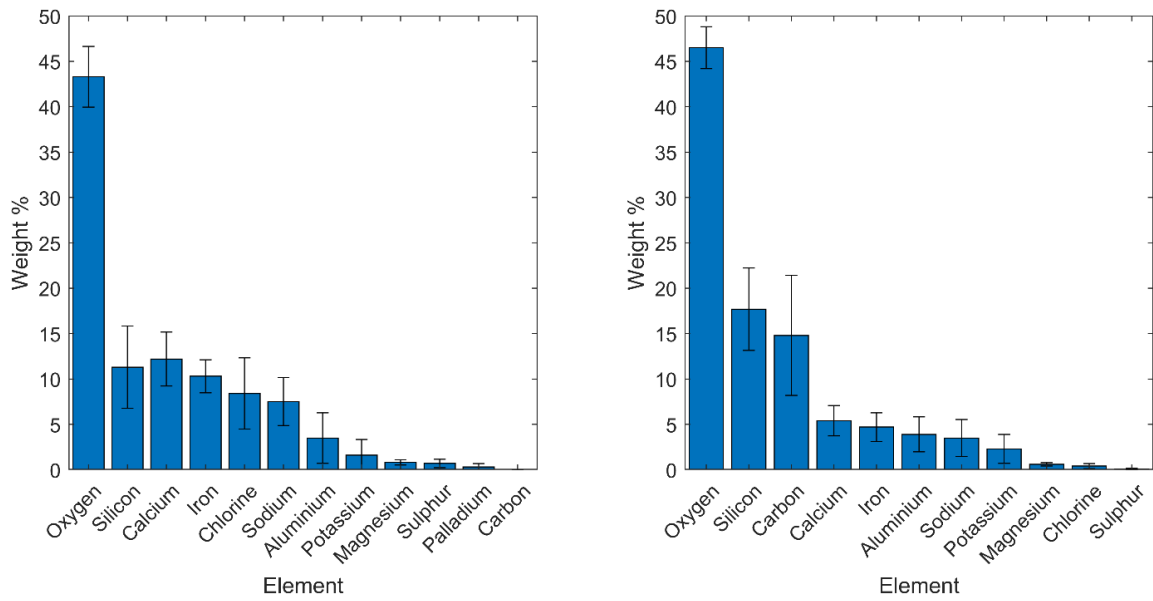


Figure 20. EDS analysis of the SP sample (left) and the P sample (right).

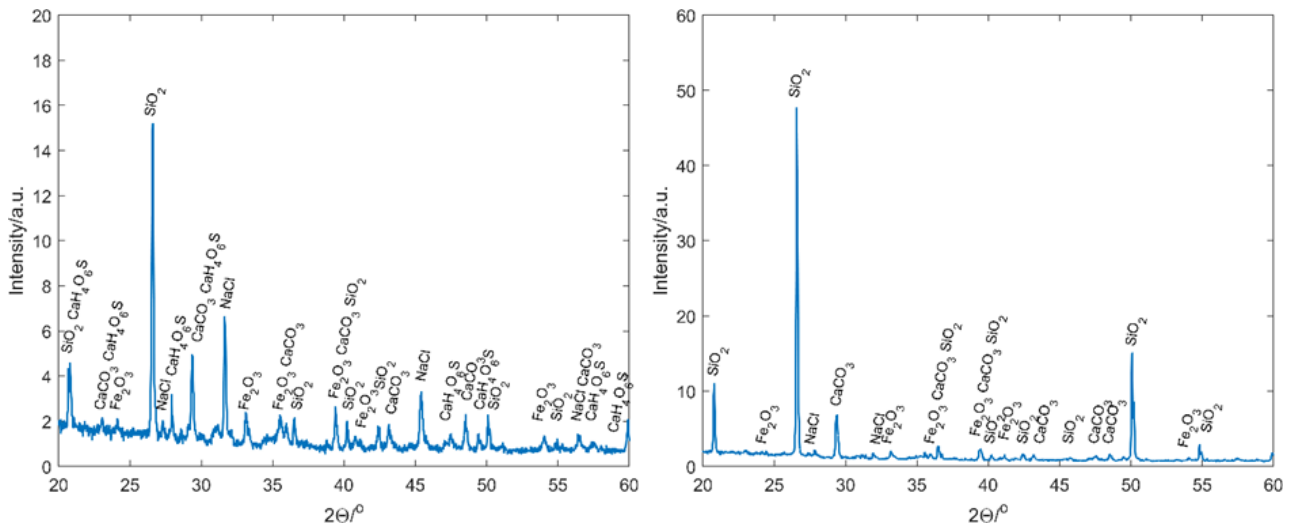


Figure 21. XRD analysis of the SP sample (left) and the P sample (right).

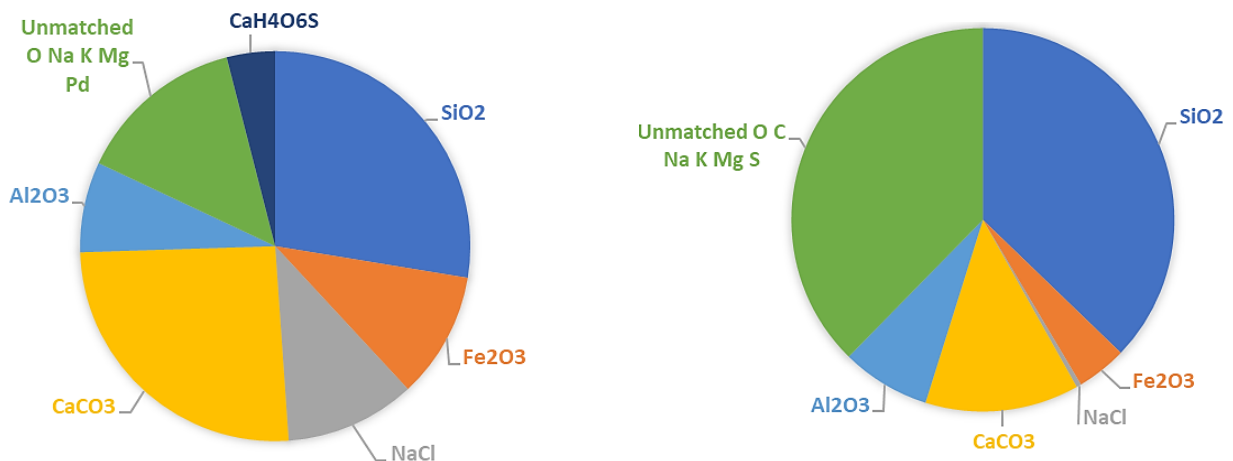


Figure 22. Likely constituents of the analysis of the SP sample (left) and the P sample (right).

The well-matched compounds are shown in Table 6 along with their more common name and the possible source of such compounds. It is immediately apparent that the identified compounds are correlated highly with the local environment. For example, at this coastal location, there is a high concentration of sand and natural salts together with building materials from the ongoing development of the university site. It is important to note, therefore, that buildings are extremely likely to observe different amounts and compositions of deposits depending on their geographical locations.

Table 6. Identified compounds and their likely sources.

Filtered Sample (P)		
Compound	Common Name	Found in/Possible Source
SiO ₂	Silicon dioxide/silica	Sand
Fe ₂ O ₃	Iron (III) oxide	Corrosion product
NaCl	Sodium chloride/‘salt’	Natural salt
CaCO ₃	Calcium carbonate	Natural salt
Al ₂ O ₃	Aluminium oxide	Corrosion product
Unfiltered Sample (SP)		
SiO ₂	Silicon dioxide/silica	Sand
CaH ₄ O ₆ S	Calcium sulphate dihydrate	Gypsum building materials
Fe ₂ O ₃	Iron oxide	Corrosion product
NaCl	Sodium chloride/‘salt’	Natural salt
CaCO ₃	Calcium carbonate	Natural salt
Al ₂ O ₃	Aluminium oxide	Corrosion product

The effect of the deposit on the conductivity of a liquid phase was also examined by producing a solution of 1% and 5% wt. deposit in deionised water, Table 7. This was carried out using the SP sample and it was found that, while the conductivity of a 1 and 5% wt. deposit solution produced lower conductivity than respective concentrations of NaCl, they did produce a solution with conductivity approximately 17 and 19 times greater than that of rainwater, respectively.

Table 7. Measured conductivity of different electrolytes.

Sample	Measured Conductivity S/m
Deionised Water	0.00
1 wt.% NaCl	2.27
1 wt.% deposit	1.65
5 wt.% NaCl	2.75
5 wt.% deposit	1.89
Tap water	0.10
Rainwater	0.10

3.5. Effect of Deposit Weight on Wetting Angle

The wetting angle exhibits a significant decrease as natural deposit is applied to the originally clean samples, as shown in Figure 23. All three paint systems when clean have similar wetting angles of approximately 65–75°, but these decrease by 35% with the addition of 4000 mgm⁻² of deposit. In the case of the PVDF and PU samples, the decrease in wetting angle appears linear with the addition of deposit; however, the PVC sample decreases more

rapidly. This clearly demonstrates that deposit built-up results in the surface becoming more hydrophilic. In practice, this would lead to less water runoff, greater spreading of the water droplets, and longer exposure times of the paint to the conductive water.

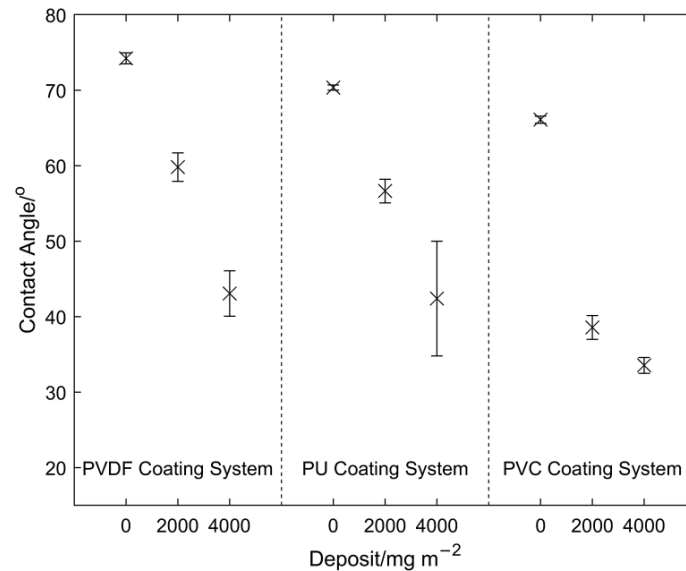


Figure 23. The effect of increased deposit build-up on the wetting angle measurements for the three different coating systems.

3.6. Effect of Deposit Weight on Water Absorption and Retention

The results of the humidity chamber test for the PVDF coating system are shown in Figure 24. It can be observed that the samples with applied deposit increased in mass through time in the humidity chamber, and that the greater the deposit weight applied, the greater this increase. The control sample gained a small amount of weight after approximately 2 h and levelled, representing some condensation due to initial sample temperature. The mean increase in mass per $\text{mg/m}^2/\text{day}$ at 95% humidity was determined to be $5 \pm 0.5 \mu\text{g}$. Thus, any surface fouling plays a key role in maintaining moisture on the paint surface, increasing water diffusion through coating to the substrate below.

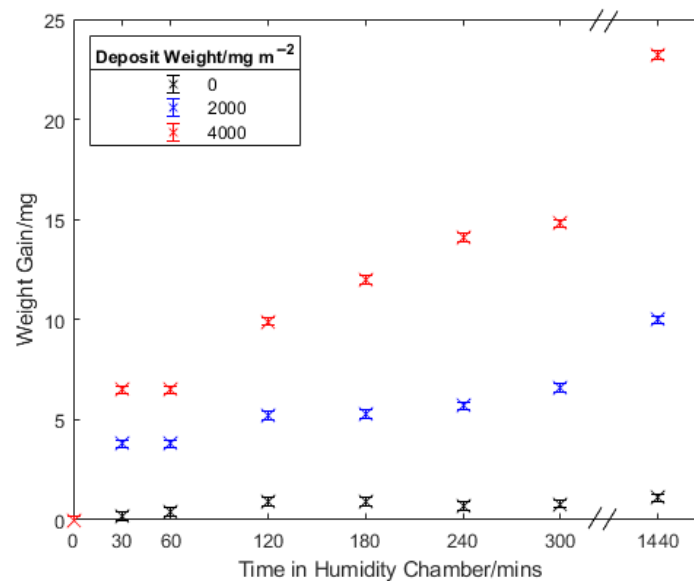


Figure 24. Water adsorption as a result of deposit weight and time in a humidity chamber for the PVDF-coated samples.

These trends were also observed with the other coating systems. For all coating systems, the weight gain with time, per mgm^{-2} of deposit vs. the clean samples, is given in Figure 25. It is displayed that all the three coating systems perform similarly, suggesting that independent of the coating system used the sample will gain approximately $4\text{--}5.5 \mu\text{g}$ of H_2O per mgm^{-2} of deposit present, per day, in a 95% humidity environment.

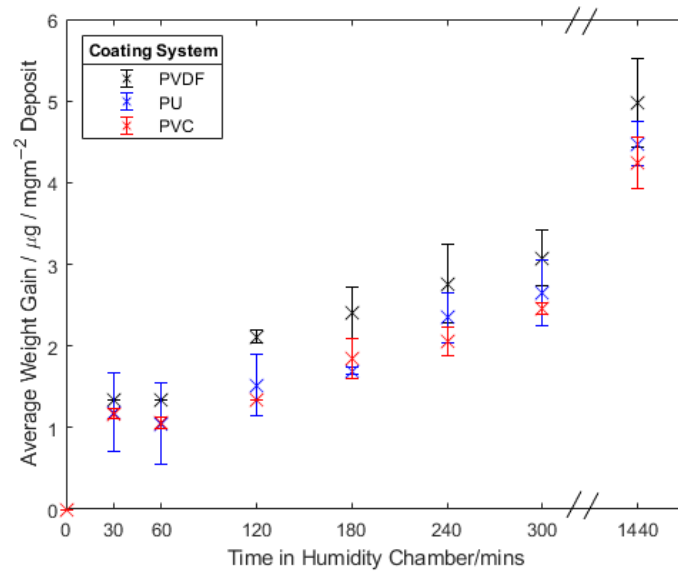


Figure 25. Water adsorption per mgm^{-2} of deposit weight as a result of time in the humidity chamber for each coating system.

When subjected to a lower relative humidity, moisture leaves the surface, Figure 26. The consistency of the mass loss suggests that the deposit build-up has little effect on the ability of the sample to dry. However, it has to be considered that the deposit-applied samples do have a reduced contact angle and hence the droplets covered a larger area. Therefore, it would be expected that the droplets on the lower contact angle samples would evaporate faster due to increased surface area to volume ratio. Hence, the fact that all the samples showed similar drying rates suggests that there is an element of the deposit retaining the water, somewhat. It is difficult, however, to conclude that amount of deposit has a significant effect on the drying rate for this sample.

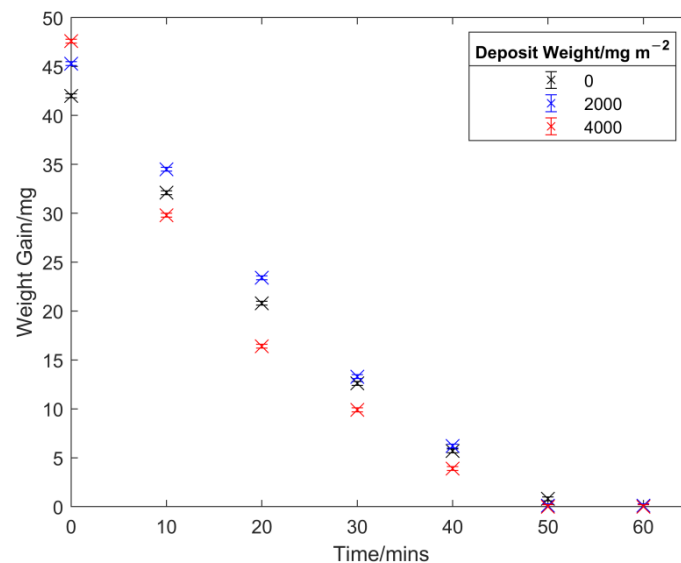


Figure 26. Effect of deposit weight on the drying of applied water droplets for the PVDF-coated samples.

Similar results were observed for the other coating systems, as shown in Figure 27. There appears to be little trend in terms of drying rate, again suggesting that the competing factors of contact angle and water retention by the deposit mean there is little difference in the drying rate observed using this testing method.

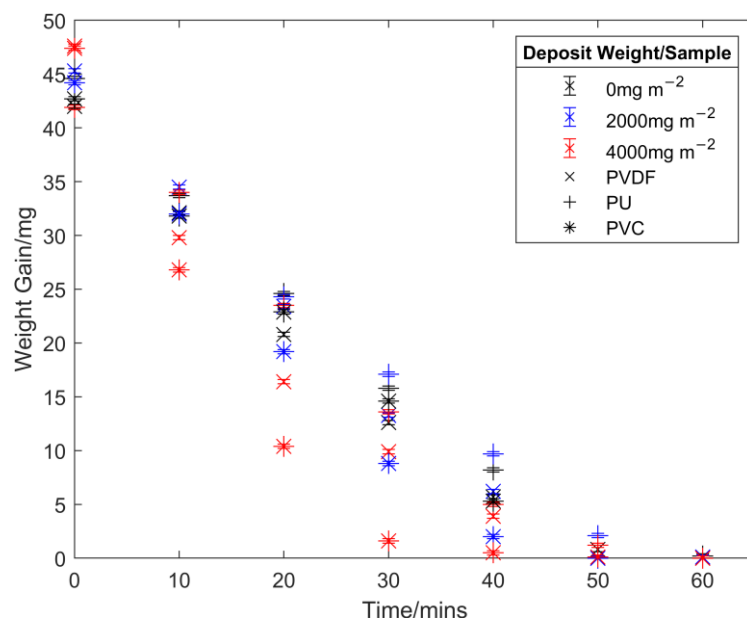


Figure 27. Effect of deposit weight on the drying of applied water droplets for all coating systems.

4. Results—Simulated Measurements

Given that the build-up of fouling deposits has been shown to be well correlated with degradation, simulations were carried out to attempt to predict locations of deposit build-up specifically by considering areas of the building that are naturally washed. These are presented along with semi-quantitative analysis and then compared to the measured fouling build-up to determine to usefulness of the model in determining the regions of fouling and therefore increased degradation concern.

4.1. Single Building Only—‘Visual’ Analysis

Simulations were carried out to understand the rain impact of each façade under different wind speeds. The contour plots discussed below show what can be considered a probability plot of the likelihood of rain particles impacting the building in each specific area, with those in blue the least likely to experience direct rain fall and those in red the most likely. Visual examination of the single building model for the east, south, and north faces, shown in Figures 28–30, shows some clearly identifiable trends.

Firstly, it is observed that the greatest barrier preventing natural washing of the façade via rain impact is the roof soffit overlap. This creates a shielded region which is protected to an extent from the wind-driven rain particles. The extent to which this occurs is a function of the wind speed; when the wind speed is low, then the sheltered area is large, but as the wind speed increases, the particle trajectory is increased in the horizontal direction reducing the sheltering effect of the roof overlap. However, even at high wind speeds of 10–12 ms^{-1} , the roof soffit still maintains a sheltering effect to some extent. At lower speeds (4–6 ms^{-1}), it is also possible to see that the doorway and window inset surrounds also produce a sheltering effect to some extent with greater sheltering observed in the higher regions of the surrounding area.

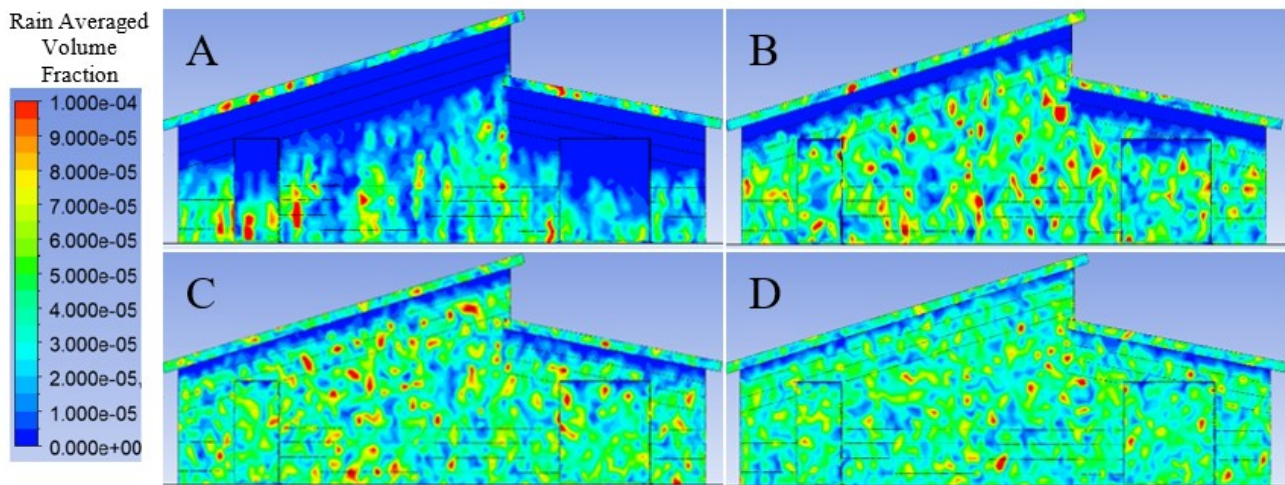


Figure 28. Predicted rain impact density for the east elevation under 2 (A), 4 (B), 6 (C), and 8 (D) ms⁻¹ wind speed applied normal to the east elevation.

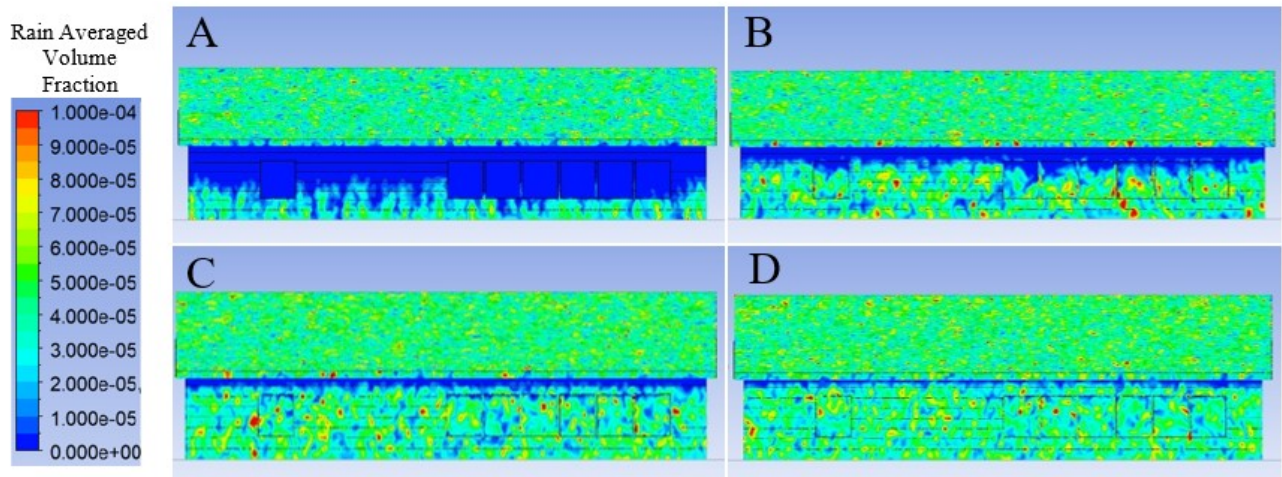


Figure 29. Predicted rain impact density for the south elevation under 2 (A), 4 (B), 6 (C), and 8 (D) ms⁻¹ wind speed applied normal to the south elevation.

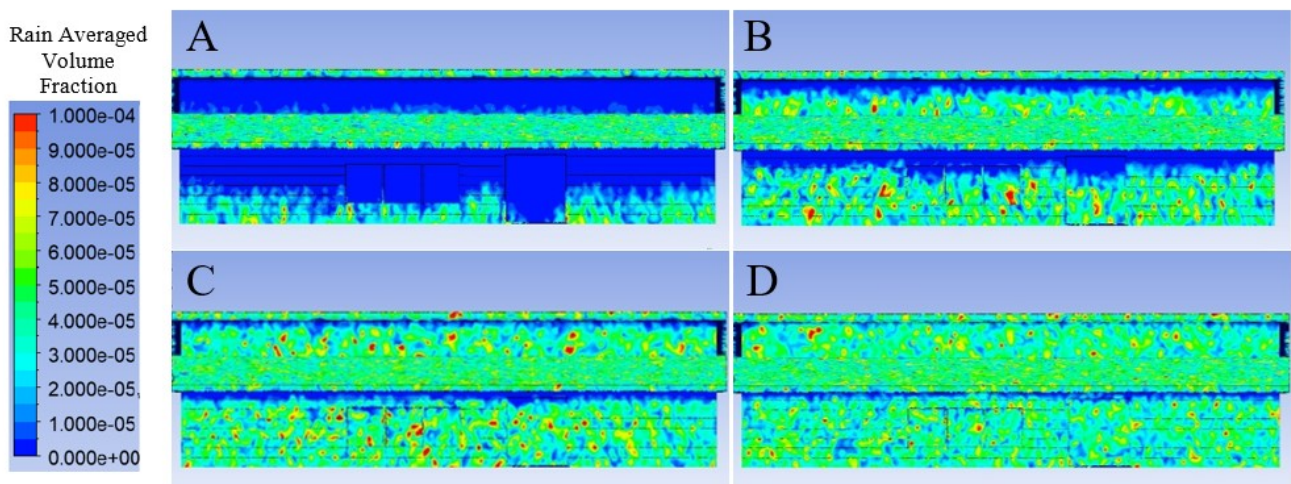


Figure 30. Predicted rain impact density for the north elevation under 2 (A), 4 (B), 6 (C), and 8 (D) ms⁻¹ wind speed applied normal to the north elevation.

It is worth noting that the regions that are shown to have a low probability of natural washing are well correlated to those that have a high quantity of natural deposits. This provided some confidence that the model may be able to predict regions likely to be subjected to fouling and therefore higher degradation rates. The exception to this is the north face where this model predicts that similar rain impact occurs on the south and north faces, suggesting that similar deposit levels should be seen on the actual building. However, this is thought to be due to the lack of the second sheltering building in this model.

4.2. Single Building Only—Semi-Quantitative Analysis

The measured average rain volume fraction for each location identified in Figure 11 can be seen in Figure 31. This provides further evidence to corroborate the visual observation that the roof soffit provides a sheltering effect that decreases with increased wind speed. It is also apparent just how significant that sheltering effect is on the higher panels (6–8), suggesting a very low probability of direct rainfall contacting these panels unless a high normal wind speed is present.

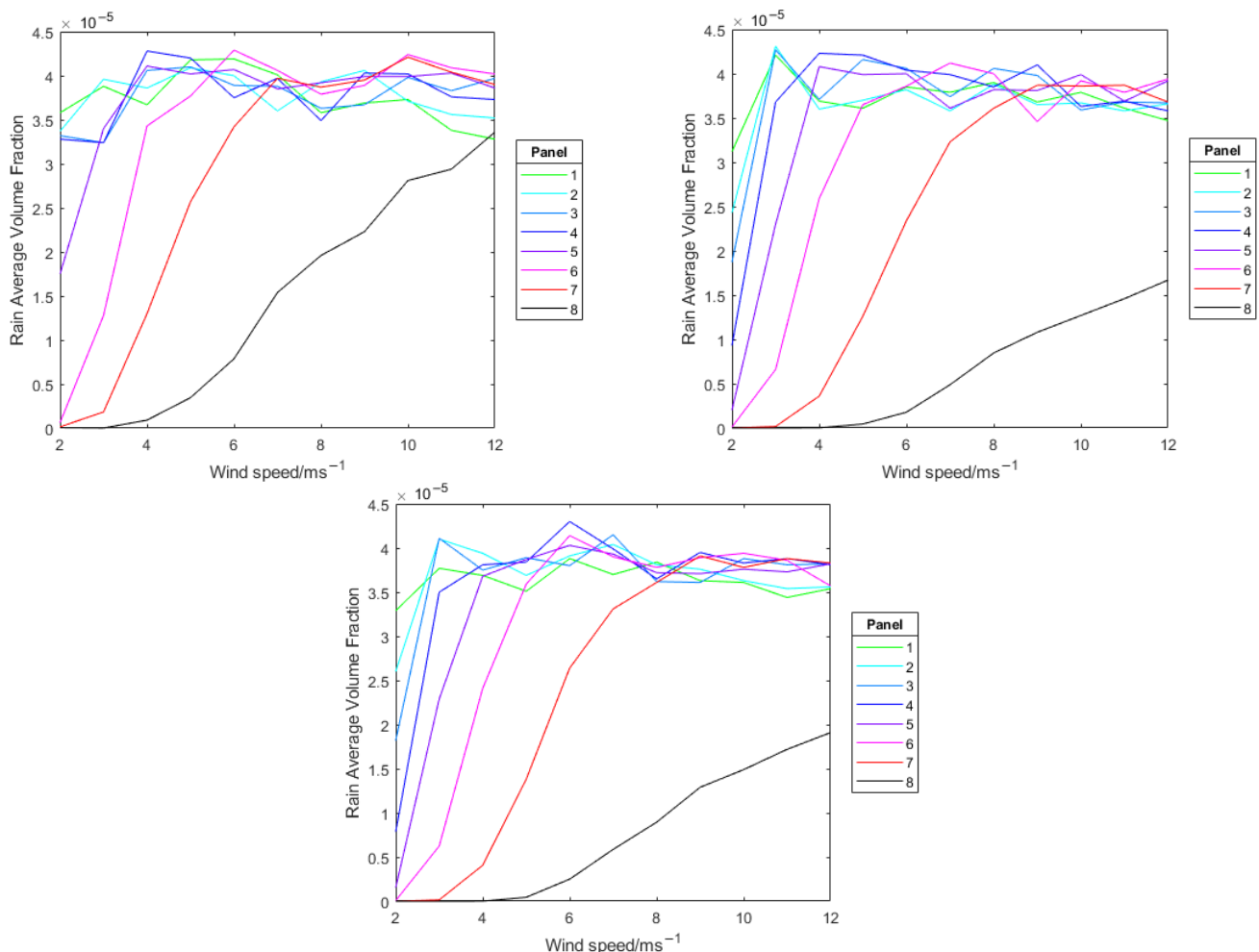


Figure 31. Measured average rain volume fraction at each location for the east (top left), south (top right), and north (bottom) façade.

In order to compare these results to the measured fouling, for each panel the values of rain average volume fraction for each wind speed were converted into a single value using a weighted average corresponding to the likely wind-speed probability shown in Figure 32. It was thought that the wind-speed probability was suitable for the location tested given the previously mentioned average weather conditions.

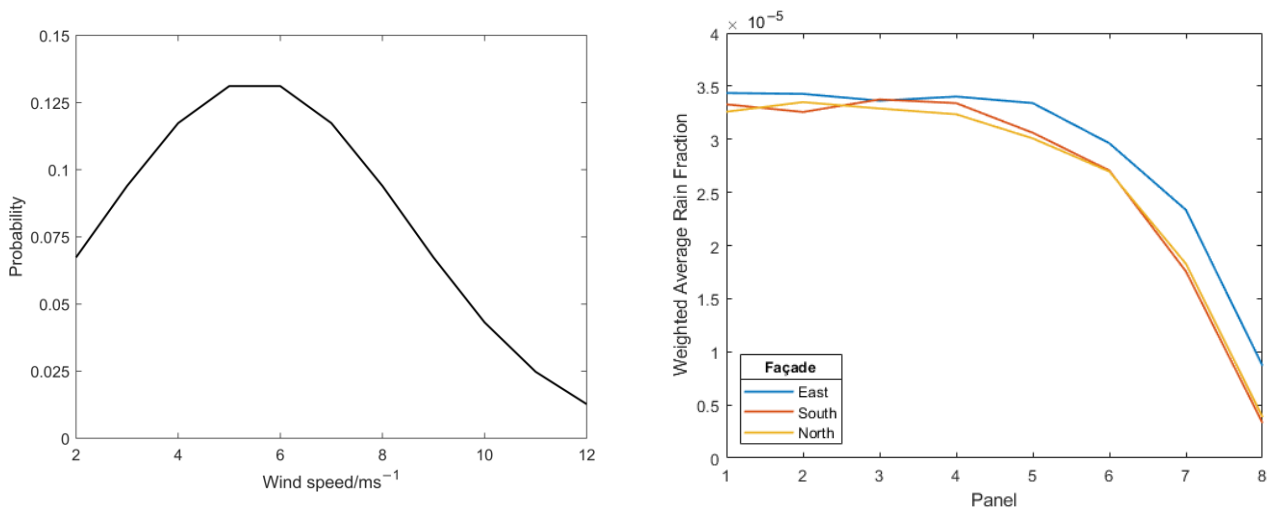


Figure 32. Wind-speed probability distribution used (left) to calculate wind-speed weighted averaged rain fraction for each panel on each façade (right).

When this value was plotted against the measured deposit fouling, Figure 33, the results show that, as expected, the extent of fouling increases as the quantity of model-predicted rain impact decreases. While the east and south faces generally show similar behaviour, the north face, however, is observed to show far greater fouling for a similar weighted average rain fraction. It is thought this is due to the importance of considering other nearby buildings on the effect of natural building washing and not solely the geometry of the building of interest.

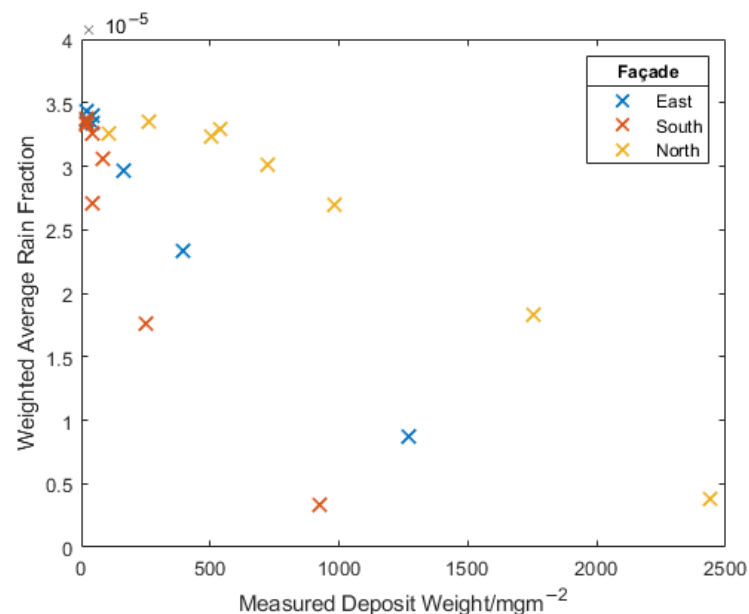


Figure 33. Comparison between measured deposit fouling intensity and model predicted rain impact density.

4.3. Adjacent Building Model—‘Visual’ Analysis

The model above provided an accurate representation of the naturally washed regions of the east and south face; however, it did not accurately represent the north face in terms of the measured deposit build-up. This was attributed to the omission of the second semi-sheltering adjacent building, which may provide a significant change to the predicted rain impact density on the north face it overlooks. The second model included this adjacent building and the resulting contour map of rain impact the north face, shown in Figure 34,

displays this effect. It is clear that, when compared to the single building model, the dual building model predicts far less natural rain impact on the north face. This correlates far better to the measured deposit build-up shown previously with high levels of deposit observed on the lower panels.

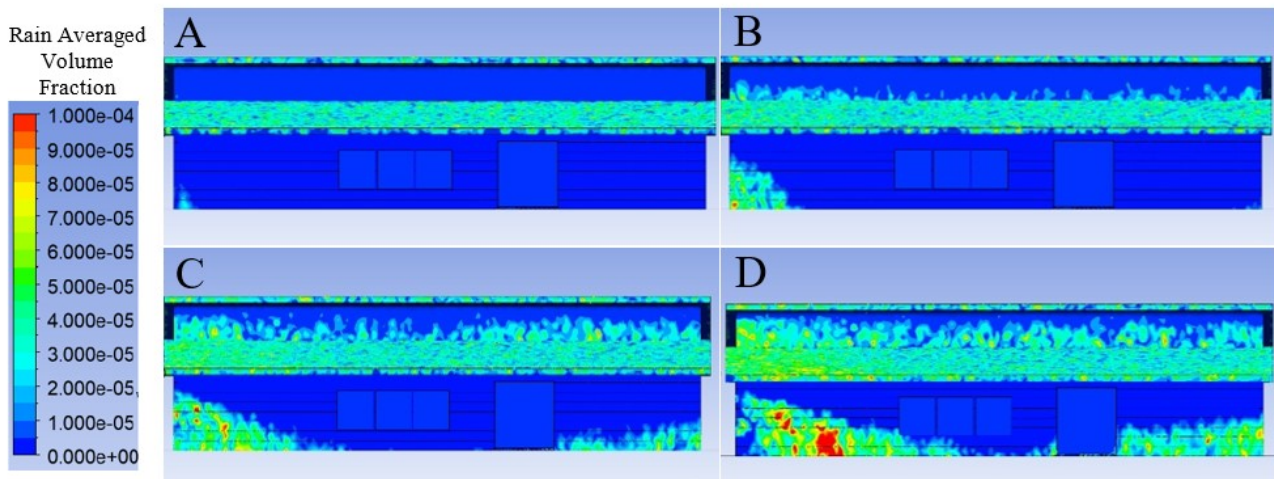


Figure 34. Effect of the semi-shielding building on the predicted rain impact density for the north elevation under 2 (A), 4 (B), 6 (C), and 8 (D) ms^{-1} wind speed applied normal to the north elevation.

4.4. Adjacent Building Model—Semi-Quantitative Analysis

It is observed in Figure 35 that with the adjacent building included in the model all the panels on the north façade record far lower averaged volume fractions of rain at the lower wind speeds ($2\text{--}8 \text{ ms}^{-1}$). In fact, it is observed that a wind speed of 8 ms^{-1} is required just for panel 1 to receive a similar rain average volume fraction to panel 1 in the single building model at just $2\text{--}4 \text{ ms}^{-1}$. While panels 1–4 do experience slightly higher volume fractions at high wind speeds $8\text{--}12 \text{ ms}^{-1}$, it should be noted that panels 5–8 never record similar volume fractions to those in the single building model, even at high wind speeds. This difference in the predicted north façade rain impact density in the two models is further shown by the wind-speed-weighted average rain fraction, also shown in Figure 35.

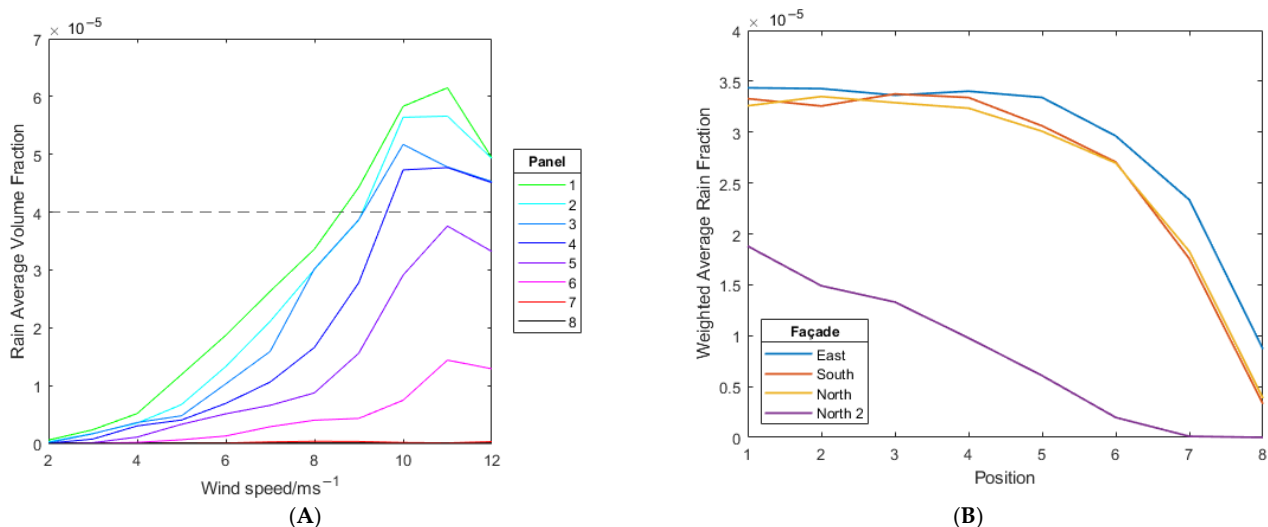


Figure 35. (A) Measured average rain volume fraction at each location for the north façade in the dual building model. The dashed line represents the maximum volume fraction achieved in the single building model. (B) Comparison between the wind-speed-weighted rain impact density for the two models used.

The improvement on the north face model by adding the adjacent building is further evidenced when again comparing the model-predicted rain impact density against the measured deposit fouling, Figure 36. When considering the trend line provided by the east and south façade data, the north façade data provided by the second (with the adjacent building) fit far better than that of the original model (without the adjacent building). These results build on the previous visual results to highlight the importance of the adjacent building on the expected natural washing of the building leading to increased deposit build-up in regions that would otherwise be considered to be naturally washed. Given the effect that natural deposit fouling appears to have on degradation, this is a significant consideration.

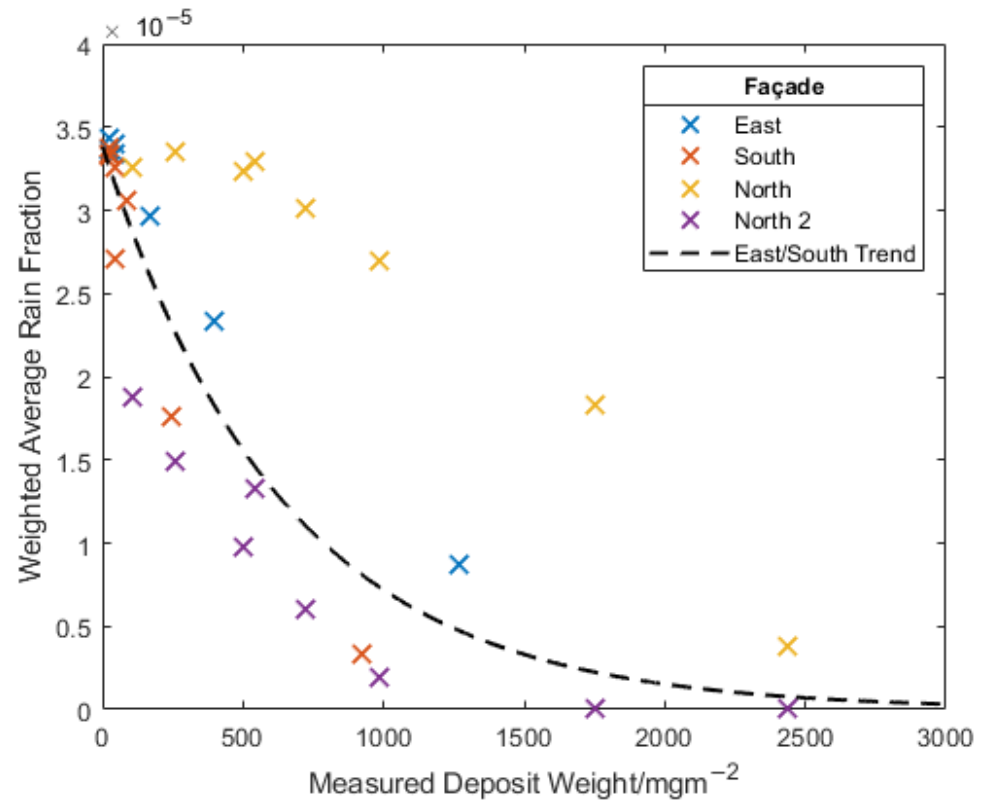


Figure 36. Comparison of the fitting of north façade data from each model to the trend given by the east and south façade data.

4.5. Using the Simulation to Predict Degradation Rates

While it is promising to see a clear correlation between the simulations and the deposit fouling intensity, the far more important factor is the measured distance of the cut edge corrosion defect. The result of plotting this against the wind-speed weighted average rain fraction for all façades and panels, Figure 37, is a highly correlated exponential trend between the two factors, providing an R^2 value of 0.94. The exponential decay of the cut edge defect distance with simulated rain fraction was thought to be explainable through the effect of cleaning and therefore the relative influence of deposits. As the rain impact density increases, the fouling decreases, which leads to an ever-smaller contribution of the fouling deposit to the degradation. This suggests the simulations could accurately be used to determine likely areas of concern.

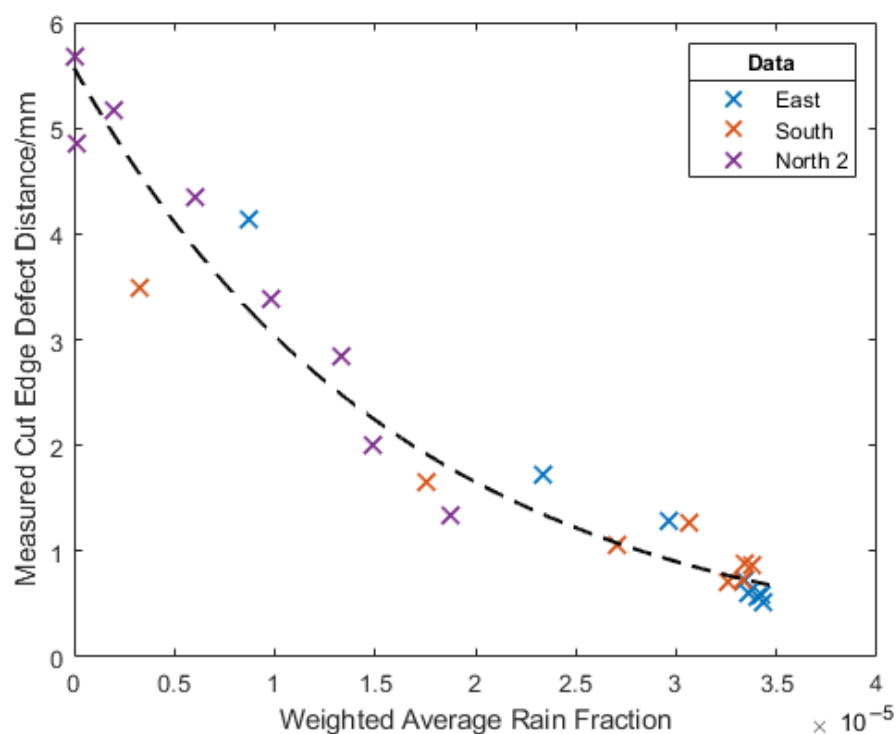


Figure 37. Comparison of measured cut edge defect distance and the model-predicted rain impact density.

5. Discussion

It was shown that significant variations in the degradation of steel architectural cladding can be experienced around a building, and that this caused by the formation of microclimates due to building geometries. Regions separated by less than 30 cm can experience significantly different degradation. What was observed in this work builds on research claims [20], that it is the more sheltered regions of the building that often receive far lower exposure to rain and sunlight, which appear to show the greatest levels of degradation. These regions generally only experience high levels of a single conventional aggressive condition—humidity; however, in the present example, it appears that OCS performance is more highly correlated with the build-up of natural fouling deposits than any other measured factor. Significantly, even regions with relatively similar humidity levels show vastly different levels of degradation when the amount of deposit is varied. Natural deposits (although usually only specifically pollutants) have been shown previously to be key accelerators of degradation for façades of other construction materials, such as paint, concrete, and ceramic [24,36,37], but have often not been examined or measured in great detail as factors when comparing discrepancies between natural and accelerated weathering of OCS [4,38].

The present investigation builds on an understanding that has emerged in the OCS research field that the unprofessional concept ‘more exposure is worse’ is outdated as the performance of coatings has improved [20]. The significant development of coating resistance to UV (requiring the new Ruv5 classification of BS EN 10169:2022 [39]) and water (5000 h+ humidity testing by BS EN 13523-25 [39]) means that generally OCS is very durable to high exposure to sun and rain, and very rarely is degradation experienced in the centre of a panel unless a significant defect, such as a scratch, is produced as a result of, for example, poor installation. Owing to this, the most commonly seen defect is caused by corrosion at the cut edge where exposure of the substrate is inevitable [19]. What is shown in this work is that cut edge corrosion occurs far faster in sheltered regions due to the increased humidity combined with aggressive salty deposits that naturally absorb water and hence maintain a highly corrosive environment. In comparison, exposed areas

frequently experience a natural cycle of washing and drying and are therefore subjected overall to less corrosive conditions.

While our work above focuses on a single building, it is important to consider generally the implications of these results on current testing methods. While sheltered regions that are not naturally washed do exist on outdoor weathering testing racks (BS EN 13523-19 [39]), due to the small size of the sample and overhang, this region is less likely to show significantly increased fouling and humidity compared to the bulk to the same extent as was measured on the present building. Furthermore, it is important to consider the highly localised nature of the deposit constituents. Depending on the weathering site used, a representative deposit may be formed; however, it is likely that the exact composition, and therefore the effect on degradation, will vary between test site and the eventual site of product use. Two of the most common testing standards for outdoor weathering, EN 13523-19 and ISO 2810, make no specification as to the debris environment and no significant recommendations are made concerning any analysis of fouling during testing except general, mostly visual, qualitative comparisons such as those described in BS EN 13523-29 [39,40]. This means that a key factor shown to be highly correlated with the degradation rate of OCS is insufficiently defined during natural exposure testing. This is similarly true for accelerated weathering tests, while there are tests for high UV and saline exposure, there is no such test for accelerated fouling-induced degradation.

Hence, it is unlikely that the determination of performance purely from standard tests is fully representative for in-service use, especially concerning regions sheltered from natural washing. Identification of where these regions occur is therefore important.

The simulation work supports this understanding of the importance of the natural washing of panels on the likely rate of fouling and therefore degradation. It was shown that an indication of sheltered regions can be created using a computational model such as the one presented here. This can, therefore, act as a simple way to determine likely areas of accelerated degradation, especially those caused by a nearby sheltering building and/or other structures. The authors believe that similar models could be used in the building design process to highlight the effect certain building geometries may have on the likely size of highly aggressive unwashed areas. While this may not be significantly important to alter building design, it could be used by the cladding supplier to highlight areas to the installation team where cladding solutions should be used that do not expose the cut edge. Furthermore, if any maintenance or inspection is to be carried out, the model could provide areas on which to focus, thus leading to reduced cost and time.

The limitations of this work are that it was carried out on a single building in a single location. The degradation effects of fouling deposits in this region were significant; however, this may not be representative of all building locations due to variations in the deposit constituents. Coastal regions will inevitably produce aggressive salty deposits, but other locations such as rural or urban may also produce deposits with other potential accelerants, such as ammonia, acid rain, or pollutants. This is noted in [38] as a possible reason for differences in electrochemical measurements of naturally weathered samples in coastal, urban, and mountainous regions. Further work is required to assess several locations to determine the aggressiveness of the deposit in each. Although the simulations did determine the areas where degradation was occurring fastest on the building considered, the investigation and simulation of other buildings of different sizes and shapes is required to determine the effectiveness and accuracy of this method.

6. Conclusions

The performance of identical OCS cladding across a building was shown to vary significantly as a result of localised environmental factors. This work agrees with other studies that show most degradation occurs at the cut edge, but reinforces suggestions that the greatest concern should be regions that are less exposed to the elements and less likely to be naturally washed.

Quantitatively, areas that were unwashed produced cut edge defects that had propagated six times farther (1 mm compared to 6 mm) into the cladding compared to those areas most naturally washed.

This work suggests this is because these regions suffer from significant build-up of locationally correlated deposits which, in coastal regions, seem to be exceptionally aggressive. Under the increased humidity also present in unwashed locations, these deposits create a wet, corrosive environment, accelerating cut edge corrosion.

In comparison, although the more exposed areas of a building are subject to higher levels of UV and rain, modern coatings are adequately durable and increased natural cleaning and drying reduces cut edge corrosion in these regions.

This work identified that sheltered regions of concern exist in the eaves of the buildings and enclosed doorways and windows, but can also be produced on a larger scale by the sheltering effect of nearby buildings.

However, it seems that fairly simple simulations of areas likely to be washed are possible, leading to the identification of areas likely to face harsher conditions. The information gathered from these simulations will allow for better design, more appropriate product deployment, and targeting of maintenance and inspection work.

Author Contributions: Conceptualisation, T.S. and E.J.; methodology, T.S. and E.J.; validation, T.S.; formal analysis, T.S.; investigation, T.S.; resources, T.S. and E.J.; data curation, T.S.; writing—original draft preparation, T.S. and E.J.; writing—review and editing, T.S. and E.J.; visualisation, T.S.; supervision, E.J.; project administration, E.J.; funding acquisition, E.J. Both authors have read and agreed to the published version of the manuscript.

Funding: The authors would like to acknowledge M2A funding from the European Social Fund via the Welsh Government (c80816), the Engineering and Physical Sciences Research Council (Grant Ref: EP/L015099/1), and Tata Steel Colors, which have made this research possible.

Data Availability Statement: All data supporting this study are provided in full in the ‘Results’ section of this paper.

Acknowledgments: The authors would like to thank Tom Dunlop for carrying out and providing the XRD analysis and Chris Griffiths for his general help with the project.

Conflicts of Interest: The authors declare no conflict of interest. The funders had no role in the design of the study; in the collection, analyses, or interpretation of data; in the writing of the manuscript; or in the decision to publish the results.

References

1. Eurofer. European Steel in Figures Statistical Guide 2021; 2020. Available online: <https://www.eurofer.eu/assets/publications/brochures-booklets-and-factsheets/european-steel-in-figures-2021/European-Steel-in-Figures-2021.pdf> (accessed on 11 November 2022).
2. TATASteel. The Confidex@Guarantee. 2022. Available online: <https://www.tatasteleurope.com/construction/services/guarantees/confidex> (accessed on 4 July 2022).
3. Deflorian, F.; Rossi, S.; Fedrizzi, L. Advanced Testing Procedures for High Performance Coatings. *J. Coat. Technol.* **2000**, *72*, 81–87. [CrossRef]
4. Deflorian, F.; Rossi, S.; Fedrizzi, L.; Zanella, C. Comparison of organic coating accelerated tests and natural weathering considering meteorological data. *Prog. Org. Coat.* **2007**, *59*, 244–250. [CrossRef]
5. Savill, T.; Jewell, E. Techniques for in situ monitoring the performance of organic coatings and their applicability to the pre-finished steel industry: A review. *Sensors* **2021**, *21*, 127. [CrossRef]
6. Buchheit, R.G. Corrosion resistant coatings and paints. In *Handbook of Environmental Degradation of Materials*, 3rd ed.; Elsevier Inc.: Amsterdam, The Netherlands, 2005; pp. 367–385. [CrossRef]
7. Tator, K.B. Coating Deterioration. In *Protective Organic Coatings*; ASM International: Novelty, OH, USA, 2015; pp. 462–473. Available online: <https://dl.asminternational.org/books/book/13/chapter/143061/coating-deterioration> (accessed on 11 November 2022).
8. Knudsen, O.; Forsgren, A. *Corrosion Control Through Organic Coatings*, 2nd ed.; Schweitzer, P., Ed.; CRC Press: Boca Raton, FL, USA, 2017.
9. Munger, C.G. Causes and Prevention of Paint Failure. In *Good Painting Practice, Steel Structures Paint Manual*; Steel Structures Painting Council: Pittsburg, PA, USA, 2014; pp. 1–21.
10. Nazarov, A.; Thierry, D. Influence of electrochemical conditions in a defect on the mode of paint corrosion delamination from a steel surface. *Corrosion* **2010**, *66*, 02500401. [CrossRef]

11. Walch, M.; Mitchell, R. Biological Aspects of Corrosion of Offshore Structures. *Nav. Res. Rev.* **1894**, *16*, 901.
12. ASTM B117-19r; Standard Practice for Operating Salt Spray (Fog) Apparatus. ASTM International: West Conshohocken, PA, USA, 2019. Available online: <https://www.astm.org/b0117-19.html> (accessed on 11 November 2022).
13. ISO 4618; Paints and Varnishes—Terms and Definitions. International Organization for Standardization: Geneva, Switzerland, 2014. Available online: <https://www.iso.org/obp/ui/#iso:std:iso:4618:ed-2:v1:en%0D> (accessed on 11 November 2022).
14. ISO 11507:2007; Paints and Varnishes—Exposure of Coatings to Artificial Weathering—Exposure to Fluorescent UV Lamps and Water. International Organization for Standardization: Geneva, Switzerland, 2007. Available online: <https://www.iso.org/standard/37489.html> (accessed on 11 November 2022).
15. Appleman, B. Predicting exterior performance of organic coatings from salt spray: Two types of errors. *J. Prot. Coat. Linings* **1992**, *135*, 6111.
16. Skilbred, A.W.B.; Arntzen, O.A.; Aamodt, T.; Løken, A. Field Testing—On the Correlation Between Accelerated Laboratory Tests and Field Testing. *Corrosion* **2019**, *2019*, NACE-2019-13154.
17. Trombetta, D. Outdoor Weathering Rack. 2016. Available online: <https://weeklypellet.com/2016/07/08/plastic-weathering-demysitfied/> (accessed on 20 April 2020).
18. Q-Lab. Q-FOG SSP & CCT Cyclic Corrosion Testers. 2020. Available online: <https://www.q-lab.com/en-gb/products/q-fog-cyclic-corrosion-chamber/q-fog-ssp-cct> (accessed on 20 April 2020).
19. Ryan, P.A.; Wolstenholme, R.P. Durability, maintenance and lifespan. In *Durability of Cladding: A State of the Art Report*; Thomas Telford Ltd.: London, UK, 1994; pp. 35–72.
20. Lebozec, N.; Thierry, D. Corrosion Performance of coil coated steel: Model buildings vs ECCA panels. In Proceedings of the 4th International Symposium on Coil Coated Steel, Paris, France, 1–5 September 2016; pp. 1–23.
21. Prosek, T.; Nazarov, A.; Thierry, D. Role of steel and zinc coating thickness in cut edge corrosion of coil coated materials in atmospheric weathering conditions; Part 2: Field data and model. *Prog. Org. Coat.* **2016**, *101*, 45–50. [CrossRef]
22. Prieto, A.J.; Silva, A. Service life prediction and environmental exposure conditions of timber claddings in South Chile. *Build. Res. Inf.* **2020**, *48*, 191–206. [CrossRef]
23. Silva, A.; Prieto, A.J. Probabilistic Approach to the Service Life Prediction of Timber Claddings. In Proceedings of the XV International Conference on Durability of Building Materials and Components (DBMC 2020), Barcelona, Spain, 20–23 October 2020.
24. Barreiras, J.; Dias, I.S.; Silva, A.; de Brito, J.; Flores-Colen, I.; Tadeu, A. Impact of environmental exposure on the service life of façade claddings—A statistical analysis. *Buildings* **2021**, *11*, 615. [CrossRef]
25. Ferreira, C.; Barreiras, J.; Silva, A.; de Brito, J.; Dias, I.S.; Flores-Colen, I. Impact of environmental exposure conditions on the maintenance of facades’ claddings. *Buildings* **2021**, *11*, 138. [CrossRef]
26. Prieto, A.J.; Silva, A.; de Brito, J.; Macias-Bernal, J.M. Serviceability of facade claddings. *Build. Res. Inf.* **2018**, *46*, 179–190. [CrossRef]
27. Ryan, P.A.; Wolstenholme, R.P.; Howell, D.M. Risk of failure. In *Durability of Cladding: A State of the Art Report*; Thomas Telford Ltd.: London, UK, 1994.
28. Adafruit. Adafruit BME680—Temperature, Humidity, Pressure and Gas Sensor. Available online: <https://www.adafruit.com/product/3660> (accessed on 7 April 2020).
29. Texas Instruments. Infrared Thermopile Sensor in Chip-Scale Package. 2012. Available online: <http://www.ti.com/product/TMP006/description> (accessed on 11 November 2022).
30. Vishay. VEML6075 Vishay Semiconductors Not for New Designs UVA and UVB Light Sensor with I2C Interface. 2019, pp. 1–11. Available online: www.vishay.com/doc?91000 (accessed on 11 November 2022).
31. Shinyei Corporation. Particle Sensor Model PPD42NS. 2010. Available online: http://www.seeedstudio.com/wiki/images/4/4c/Grove_-_Dust_sensor.pdf (accessed on 11 November 2022).
32. Bunaciu, A.A.; Udriștioiu, E.G.; Aboul-Enein, H.Y. X-ray Diffraction: Instrumentation and Applications. *Crit. Rev. Anal. Chem.* **2015**, *45*, 289–299. [CrossRef] [PubMed]
33. EngineeringToolBox. Air—Density, Specific Weight and Thermal Expansion Coefficient vs. Temperature and Pressure. 2003. Available online: https://www.engineeringtoolbox.com/air-density-specific-weight-d_600.html (accessed on 21 June 2022).
34. EngineeringToolBox. Drag Coefficient. 2004. Available online: https://www.engineeringtoolbox.com/drag-coefficient-d_627.html (accessed on 21 June 2022).
35. Kubilay, A.; Derome, D.; Blocken, B.; Carmeliet, J. CFD simulation and validation of wind-driven rain on a building facade with an Eulerian multiphase model. *Build. Environ.* **2013**, *61*, 69–81. [CrossRef]
36. Grøntoft, T. Estimation of damage cost to building facades per kilo emission of air pollution in Norway. *Atmosphere* **2020**, *11*, 171. [CrossRef]
37. Sousa, V.; Almeida, N.; Meireles, I.; De Brito, J. Anomalies in wall renders: Overview of the main causes of degradation. *Int. J. Archit. Herit.* **2011**, *5*, 198–218. [CrossRef]
38. Deflorian, F.; Rossi, S.; Fedel, M. Organic coatings degradation: Comparison between natural and artificial weathering. *Corros. Sci.* **2008**, *50*, 2360–2366. [CrossRef]

39. *BS EN 13523*; International Standard—Coil Coated Metals. Test Methods. BSI: London, UK, 2020. Available online: <https://www.bsigroup.com/en-GB/> (accessed on 11 November 2022).
40. *ISO 2810:2020*; Paints and Varnishes—Natural Weathering of Coatings—Exposure and Assessment. International Organization for Standardization: Geneva, Switzerland, 2020. Available online: <https://www.iso.org/standard/76042.html> (accessed on 11 November 2022).

Disclaimer/Publisher’s Note: The statements, opinions and data contained in all publications are solely those of the individual author(s) and contributor(s) and not of MDPI and/or the editor(s). MDPI and/or the editor(s) disclaim responsibility for any injury to people or property resulting from any ideas, methods, instructions or products referred to in the content.